# Medium Modifications of Vector Mesons in the Subthreshold Region

G.J. Lolos, Z. Papandreou, E.J. Brash, G.M. Huber, R. Lewis,
K. Benslama, S. Dumalski, A. Fleck, N. Knecht, A. Shinozaki
*Department of Physics, University of Regina, Regina SK S4S 0A2, Canada*

P.L. Cole
*Department of Physics, University of Texas at El Paso, El Paso TX 79968*

F.J. Klein and S.G. Stepanyan
*Thomas Jefferson National Accelerator Facility, Newport News, VA*

N. Bianchi, E. De Sanctis, M. Mirazita, V. Muccifora, F. Ronchetti, P. Rossi
*INFN-LNS, via E. Fermi 40, I-00044 Frascati, Italy*

M. Anghinolfi, M. Battaglieri, P. Corvisiero, M. Ripani, M. Taiuti
*INFN-Sezione di Genova e Dipartimento di Fisica dell' Università, I-16146 Genova, Italy*

K.Sh. Egiyan, G. Gavalian and Y.G. Sharabian
*Yerevan Physics Institute, Yerevan 375036, Armenia*

B. Raue
*Florida International University, Miami, FL 33199*

A. Afanasev
*Dept. of Physics, North Carolina Central University, Durham, NC*

B.K. Jennings
*TRIUMF, 4004 Wesbrook Mall, Vancouver, British Columbia, Canada V6T 2A3*

M. Khandaker
Norfolk State University, Norfolk, VA 23504

D.S. Carman
Ohio State University, Athens, OH 45701

May 21, 1999

**Abstract**

We propose to investigate the subthreshold photoproduction of the three lowest mass vector mesons, $V = \rho^0$, $\omega$, and $\phi$. In the subthreshold energy region, defined here as the energy region below the $\gamma + N \to V + N$ reaction threshold on the free nucleon, VMD-driven vector meson production is suppressed and the influence of hadronic matter on the masses of the vector mesons is emphasized. This method is the optimum vehicle for the study of in-medium modifications and, specifically for the $\rho^0$ meson, experimental evidence already exists for a dramatic reduction in $m_{\rho^o}$, which is dependent on the incident photon energy or the $\rho^0 - N$ relative momentum. Different regions of phase space may be more sensitive to different reaction mechanisms and this assertion will be tested for the $\rho^0 \to \pi^+\pi^-$ channel, and the study will be extended also to the unexplored domains of the $\omega \to \pi^+\pi^-\pi^0$ and $\phi \to \pi^+\pi^-\pi^0$ vector mesons. In addition, the hypothesis of vector mesons forming bound states in nuclei will be explored.

An effective nuclear target for this investigation is $^3He$. The minimum trigger requirement is the detection of two charged particles (with an open neutral trigger). We request 420 hours of nominal tagger photon beam ( $10^7\gamma/s$ ) in Hall B, in the tagged photon region between 320 MeV and 1520 MeV, of which 150 hours can be collected in the already approved *g3* period.

**Nature of the Update in this Proposal**

This proposal is an update (modification) to E99-001, which was deferred by PAC15. The changes, which address the issues raised by PAC15, have been incorporated into Sections 4 and 5. These two sections are **critical** in understanding the proposed analysis with CLAS, leading to the final extraction of medium induced mass and width modifications of the vector mesons. Other changes to the proposal consist mostly of trimming and rearranging. The conclusions, physics objectives, beam time request, and methodology remain the same as those in the original E99-001, thus, in every aspect, this is an update not a new proposal.

**This is a Hall B Collaboration experiment.**

# 1 Scientific Motivation

Recently, much attention has been directed to the coupling of vector mesons to nucleons, especially under conditions of high nuclear matter density where it is expected that this coupling will be modified in comparison to the situation on an unbound nucleon. Clearly, the $\rho^0 - N$ coupling in nuclei, for example, must be known accurately as it is an important ingredient in the calculation of the $N - N$ interaction.

Examples of this interest in vector mesons range from $e - A$ and $\gamma - A$ physics at Jefferson Lab, to relativistic heavy ion collision experiments at CERN, GSI and in the future at RHIC (with an implication on the transition from normal hadronic matter to the conjectured but elusive quark-gluon plasma [1]). The latter has cosmological significance, since the universe was in this deconfined phase a few microseconds after the Big Bang. Other fields of interest include the determination of the equation of state for nuclear matter in connection to the underlying mechanism of supernovae explosions [2] and the properties of remnant neutron stars [3]. All the experiments above involve effects in systems which transit from nucleonic to quark degrees of freedom.

A transition of this nature occurs already in normal nuclear matter. Our aim is to photoproduce the light vector mesons *in the interior* of the nucleus, below the free production threshold, by exploiting the Fermi momentum of nucleons. We will demonstrate that this is the most direct method in the study of in-medium vector meson coupling.

## 1.1 Theoretical Overview

The interior of a nucleus belongs to the long-range and non-perturbative transition region of QCD, which is largely unexplored. Here, QCD-driven interactions among nuclei and mesons affect fundamental particle properties such as masses, lifetimes, and coupling constants. At high hadronic matter temperatures, $T \sim 150$ MeV, lattice QCD calculations [4] support the expectation that the scalar quark (chiral) condensate $< \bar{q}q >$ vanishes, an effect which signifies the transition of nuclear matter from a spontaneously broken symmetry phase to a chirally restored one. However, the condensate itself is not an experimental observable, and therefore other physical quantities associated with it need to be measured to test hadronic medium effects. The masses of the light vector mesons are excellent candidates for this task.

The theoretical basis for mass modification of hadrons in the nuclear medium is overwhelming. Various theoretical methods have been employed in this effort: QCD sum rules ($QSR$), chiral pertubation theory ($\chi PT$), quark-meson coupling ($QMC$) model, effective Lagrangian theories, Nambu-Jona-Lasinio models, etc. Several review articles have appeared in print on this topic recently [5, 6, 7], and the reader is referred to the significant number of publications therein. Even though either high temperature $T$ or high nuclear matter density $\rho_{nuc}$ will result in vector meson

mass modification, there are significant differences between these two conditions. For the mass modification to take place, the hadronic medium temperature must approach a critical temperature $T_c \sim 150$ MeV [8, 9]. On the other hand, while chiral restoration is expected to take place at nuclear matter densities $\rho \geq 5\ \rho_{nuc}$ [7], substantial changes in the $< \bar{q}q >$ condensate (of $\sim 30\%$) can take place even at normal nuclear matter densities, $\rho_{nuc} = 0.16$ fm$^{-3}$. This transition occurs when the scalar field energy reaches a value of 250 MeV/fm$^3$, which corresponds to an energy density of $\epsilon = 1$ GeV/fm$^3$ [8]. Such a density can be reached in heavy ion collisions or *inside a nucleon*. Clearly, experiments probing such density effects stand to yield valuable information.

The effect of mass modifications on hadrons has been postulated [10]. This is the original scaling argument by Brown and Rho, who predict that the masses of other light vector mesons scale approximately like those of hadrons:

$$m_N^*/m_N \sim m_\sigma^*/m_\sigma \sim m_V^*/m_V \sim f_\pi^*/f_\pi \tag{1}$$

where the $*$ denotes the medium-modified quantities.

Numerical predictions for the $m_V^*/m_V$ ratio have been produced by a large spectrum of other models. It should be noted that most authors treat the $\rho^0$ and the $\omega$ in the same manner, whereas they quote a different modification for the $\phi$ meson. The latter is of particular interest since it is modulated by the strangeness content of the nucleon ($OZI$-breaking parameter), $y = 0.1 - 0.2$, in QCD [11, 12]. The modified masses obey the following relations:

$$m_{\rho,\omega}^*/m_{\rho,\omega} = 1 - (A \pm \delta A)(\rho/\rho_{nuc}) \tag{2}$$

$$m_\phi^*/m_\phi = 1 - (B \pm \delta B)y(\rho/\rho_{nuc}) \tag{3}$$

where

$$y = 2 < \bar{s}s >_N \ / < \bar{u}u + \bar{d}d >_N \tag{4}$$

and the quantities $A$, $\delta A$, $B$ and $\delta B$ are shown in Table 1.

The different calculations are in relatively good agreement as far as the $\rho^0$ and the $\omega$ are concerned, with an average decrease of $\sim 20\%$ predicted, at $\rho = \rho_{nuc}$. A smaller result is predicted for the $\phi$ [13, 14], although not all authors agree [16]. Nevertheless, a consensus appears to be emerging from the theoretical community that the masses of the light vector mesons will decrease in nuclear matter, but the extent of the mass modification is still an open question. Finally, the width of the vector mesons was also found to decrease in *QSR* [14, 17], as the density increases: for the $\rho^0$ this implies that the phase space suppression from the $\rho^0 \to \pi^+\pi^-$ process overcomes the collisional broadening at finite density, while an opposite result has been concluded by the work of Klingl et al. [18] who find a large width increase and a small mass change.

Table 1: Vector Meson Mass Decrement. The uncertainties in the calculations arise from the density dependence of the condensates.

| Theoretical Prediction | | $m^*_{\rho,\omega}/m_{\rho,\omega}$ | | $m^*_\phi/m_\phi$ | |
|---|---|---|---|---|---|
| Model | Reference | $A$ | $\delta A$ | $B$ | $\delta B$ |
| $QSR$+Walecka | [13] | 0.16 | 0.06 | 0.15 | 0.07 |
| $QSR$+MC | [14] | 0.22 | 0.08 | 0.06 | 0.07 |
| $QMC$ | [15] | 0.17 | | | |
| Average | | 0.18 | | 0.11 | |

The medium modifications described above assume that the vector mesons are on-shell and free (in flight) within the nuclear medium. Very recently, however, another source of mass modification has been postulated, namely that of bound states of the vector mesons in nuclei, in the context of quantum hadrodynamics ($QHD$) [19]. This theory has met with considerable successes in describing nuclear charge distributions and spin observables in proton-nucleus scattering [20, 21, 22], and involves large scalar ($S$) and vector ($V$) fields in the nucleus. These deeply attractive and repulsive fields, respectively, largely cancel out, and their superposition gives rise to the typical nuclear attractive potentials. Nucleons are sensitive to both $S$ and $V$ fields, thus they cannot realize the individual deep field components.

Vector mesons, on the other hand, couple only to $S$ fields and if the vector meson kinetic energy is below that of the binding energy between it and the scalar field, a bound state is formed, and its mass is reduced by the same amount as the binding energy. A recent calculation [23], which is based on the $QMC$ model [15], predicts a large mass modification of the $\omega$, even for as light a nucleus as $^6He$, by the formation of an $\omega$-$^6He$ bound state. Furthermore, a different calculation based on $QHD$ and assuming Brown-Rho scaling, as in equation (1), resulted in a large binding energy of the $\rho^0$ in $^3He$. The resultant mass reduction agrees well with experimental results, thus providing evidence that the first such vector meson bound states may have been observed [24].

The physics origins of *bound* vector meson states in nuclei are different than the corresponding ones for mass and/or width modifications expected by the interaction of *free* $\rho^0$ and $\omega$ mesons in the interior of nuclear matter. In general, the expected mass modification for bound states is larger than those predicted for the free interaction, at least for normal nuclear matter densities. It is possible, of course, that both phenomena occur in nuclei and this may complicate the interpretation of experimental results.

Finally, a recent theoretical work has found that a proper accounting for the tensor coupling in the $\rho^0 - N$ interaction results in a substantial reduction of the $\rho^0$ mass in the nuclear medium [25]. This result is in general agreement with the results in reference [24]. The tensor coupling can be incorporated within either $QSR$

or $QHD$ based frameworks.

*It is clear that vector meson modifications are expected in some form or another, and while theoretical calculations appear to cover the whole spectrum of possible mass and width modifications, critical experimental input is urgently needed.*

## 1.2 Experimental Evidence for Medium Modifications

### 1.2.1 Hadronic Probes

There has been a flurry of recent experimental results from a number of accelerator facilities, employing hadronic probes, which have found evidence of a modified $\rho^0$ meson mass in the nuclear medium. The most notable are: heavy ion collision experiments at CERN, which have seen an unexpected enhancement in dilepton invariant mass spectra at low invariant masses [26, 27, 28]; $K^+ -^{12} C$ elastic cross section measurements at 800 MeV/c that have also revealed an enhancement which may be attributed to a shifted $\rho^0$ mass [29]; and a $\vec{p} - A$ scattering experiment at IUCF that has evoked shifted meson masses in an attempt to explain spin-transfer observables [30]. Although these types of experiments have inferred the presence of medium modifications, they were not entirely conclusive, as other conventional mechanisms could also explain the data, at least in part.

### 1.2.2 Photon Probes

The first "direct" measurement of the $\rho^0$ mass modification was performed at INS-ES, via the photoproduction reaction $^3He(\gamma_t, \rho^0 \rightarrow \pi^+\pi^-)$, with tagged photons in the energy range 800-1120 MeV and with the two pions detected in the TAGX[1] magnetic spectrometer. The analysis was consistent with a 17% reduction in the $\rho^0$ mass [32], which is illustrated in Fig. 1. A subsequent reanalysis of older TAGX double-pion production results, at lower tagged photon energies (380-700 MeV), confirmed the large mass shift [33].

The large shift extracted out of a complicated and model dependent analysis has been independently corroborated by the $p$-wave distribution of the $\rho^0 \rightarrow \pi^+\pi^-$ decay shown in Fig. 2 [34]. This $p$-wave signature only manifests itself in the 500-600 and 600-700 MeV/c$^2$ invariant mass regions, as seen in panels (b) and (c) of this figure, clearly indicating that the mass of the $\rho^0$ is shifted from its free value of 770 MeV/c$^2$, which would populate primarily the 700-800 MeV/c$^2$ bin. Since only the $\rho^0$ decays into two pions in a relative $l = 1$ state, Fig. 2 is a fingerprint of the $\rho^0$ in the data.

This figure is the result of just a single selection criterion (cut) imposed on the $\pi^+\pi^-$ data set: that the relative opening angle $\theta_{\pi\pi}$ between the two pions exceeds $70^o$. This enhances the ratio of pions from the $\rho^0 \rightarrow \pi^+\pi^-$ decay, compared to all the other $\pi^+\pi^-$ producing processes; for the latter, the angle between two uncorrelated pions does not carry a particular signature by the transformation from the

[1]For the interested reader, a detailed description of the TAGX System is presented in reference [31].

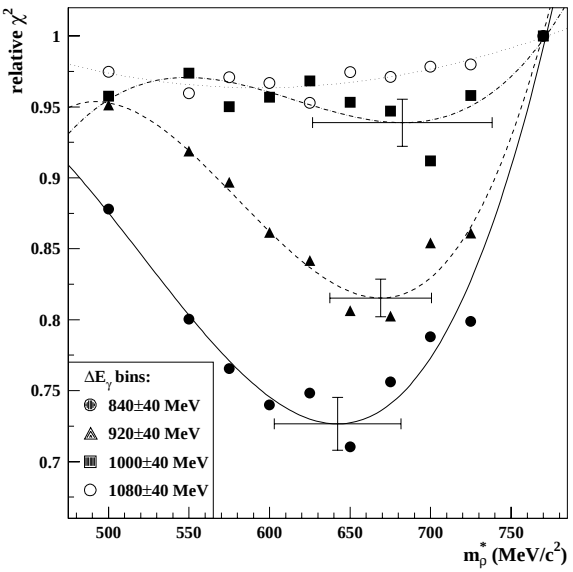


Figure 1: The dependence of the $\chi^2$ as a function of $m^*_{\rho^o}$, resulting from the MC fitting to the data [34], for four different tagged photon energy bins. The MC calculations are indicated as points, and the curves display third-order polynomial fits to these points. The extracted masses from the two lowest curves are 642±40 MeV/c$^2$ and 669±32 MeV/c$^2$ for the 800-880 MeV and 880-960 MeV tagged photon energy bins, respectively.

center-of-mass to the laboratory frame. It should be emphasized here that among all processes leading to production of two pions, *only* the $\rho^0 \to \pi^+\pi^-$ reaction populates the regions $|\cos\theta^*_{\pi^+}| \geq 0.7$, in any significant strength, and the shapes of the distributions in Fig. 2 are very well reproduced and understood by MC simulations, including the effects of the TAGX acceptance. Our MC simulations, together with TAGX data, confirm that the $\theta_{\pi\pi}$ cut does not in anyway induce a $p$-wave signature in the remaining background. *The p-wave signature and its implications, in addition to the MC-based multiparameter analysis in [34], are extremely important ingredients in the conclusions and will be expanded upon in Section 4.2.1.*

The conclusions from reference [32] were that the reduction, $\delta m_{\rho^0}$, of the $\rho^0$ mass was much larger than any theoretical prediction, and that the mass shift increased as the experiment probed deeper below threshold. This analysis will be discussed in further detail in Section 4.1, as it will form the basis for the analysis of the experiment proposed here. It is of interest to note that these conclusions are very consistent with an analysis of total photoabsorption cross sections [35], in terms of shadowing effects in nuclei, which can also be interpreted in terms of large $\delta m_{\rho^0}$.

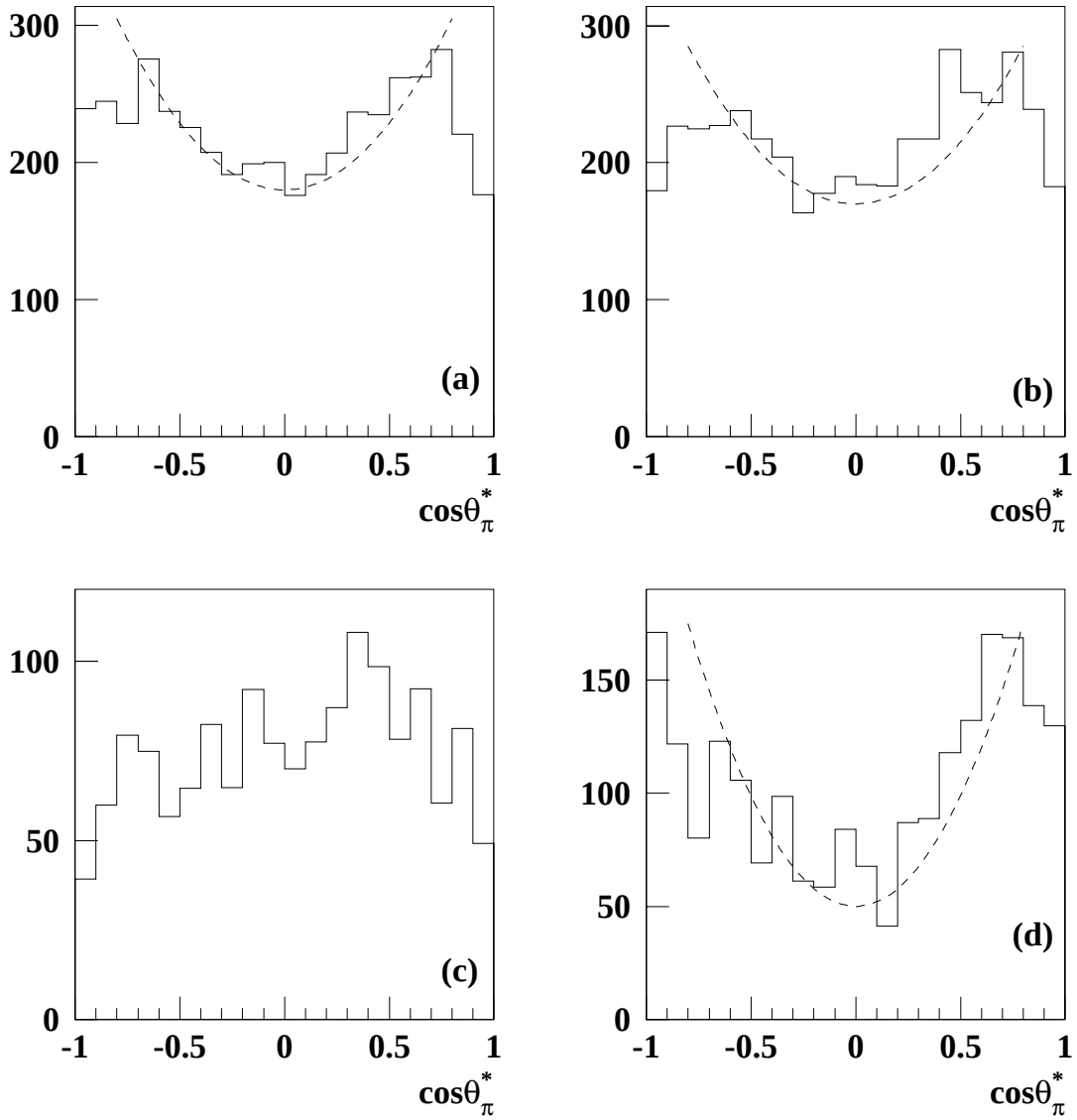


Figure 2: The $\cos\theta^*_{\pi^+}$ distribution is shown in the invariant mass regions of (a) 500-600 MeV/c$^2$, (b) 600-700 MeV/c$^2$, (c) 700-800 MeV/c$^2$ and (d) 500-600 MeV/c$^2$ after a subtraction of the "$\rho^0$ -free" 400-500 MeV/c$^2$ distribution. Panels (a), (b) and (d) capture the $l = 1$ signature of the $\rho^0 \to \pi^+\pi^-$ decay.

# 2 Physics Objectives of this Proposal

The principal properties of the three lowest mass vector mesons are displayed in Table 2, with the boxed numbers indicating the decay modes that will be measured in this experiment.

Table 2: Vector Meson Properties

| Particle ($MeV/c^2$) | Width ($MeV/c^2$) | $c\tau$ fm | BR( $\pi^+\pi^-$ ) % | BR($3\pi$) % | BR($\rho\pi$) % | BR( $e^+e^-$ ) % |
|---|---|---|---|---|---|---|
| $\rho^0$ (770) | $\sim 151$ | 1.3 | $\boxed{\sim 100}$ | $< 1.2 \times 10^{-2}$ | - | $4.5 \times 10^{-3}$ |
| $\omega$ (782) | $\sim 8.5$ | 24 | 2.2 | $\boxed{\sim 89}$ | - | $7.1 \times 10^{-3}$ |
| $\phi$ (1020) | $\sim 4.5$ | 45 | $8 \times 10^{-3}$ | $\boxed{2.5}$ | $\boxed{\sim 13}$ | $3 \times 10^{-2}$ |

We begin by stating the aims behind the study of each of these mesons. We stress that different emphasis and priority is placed on each meson, with the $\rho^0$ and $\omega$ comprising the main objectives of our study, as will be explained in detail below.

- *The $\rho^0$ meson:* We seek to provide quantitative and definitive information on the physics origin of the downward shift of the mass of this meson and a first measurement of $\delta\Gamma_{\rho^0}$ in the nuclear medium. Clearly, since the $\rho^0$ has a short decay length, its populated phase space related to medium modifications will be large, which implies that any modifications measured will carry high confidence. However, due to the large width, $\Gamma_{\rho^0}$, of this resonance and the broad shapes of competing mechanisms, and depending on the invariant mass binning that can be achieved, the experiment may be sensitive only to a change $\delta\Gamma_{\rho^0}$ of 20 $MeV/c^2$ or higher. Thus, we will be able to distinguish among theoretical models with definitive predictions on the magnitude of $\delta\Gamma_{\rho^0}$.

- *The $\omega$ meson:* This particle has not been investigated experimentally, as far as medium modifications are concerned. Whereas some models expect the $\rho^0$ and $\omega$ masses to be similarly modified [11, 14], others predict a smaller mass decrease for the $\omega$ [36]. Furthermore, the small width of the $\omega$ and its three-pion decay mode is a unique signature among mechanisms in its mass range and establishes it as a sensitive probe of even small mass and/or width modifications. This comes at the expense of reduced in-medium decay probabilities, which, with some care, can be enhanced in selected regions of phase space.

  It is, however, the investigation of the bound state of vector mesons in nuclei which places additional emphasis on the photoproduction of the $\omega$ meson. A bound $\omega$ will result in nearly 100% in-medium decay probability *if produced with very small kinetic energy with respect to the nucleus.* The long in-flight

decay length of the free $\omega$ in the nucleus, even at very low kinetic energies, will result in a small number of modified $\omega$ mesons, in contrast to the bound $\omega$ case. Thus, the observed fraction of modified to unmodified detected $\omega$ mesons will separate these two different effects. Furthermore, unlike the in-flight modifications which have an energy dependence as a function of effective $\gamma\beta c\tau$, bound states exhibit more or less a *threshold* type of energy dependence as either bound or free $\omega$ mesons within the nuclear $S$ field. Under these conditions, the $\omega$ is an ideal vehicle to probe such bound states.

- *The $\phi$ meson: QSR* predict a decrease in the $\phi$ mass, which is further modulated by the strangeness content of the nucleon (see equations (3) and (4)). In addition, as a pure $\bar{s}s$ state, the $\phi$ is sensitive to the $< \bar{g}g >$ gluon condensate, and thus the scope of medium modifications is expanded by including gluonic contributions to the interaction matrix elements [37]. Unfortunately, the populated phase space production of the $\phi$ is very small, and whether it is realistically measurable depends on the statistics we will be able to accumulate in remote regions of phase space. The drawbacks notwithstanding, the physics motivation of $\phi$ mass modifications is compelling enough to warrant a serious look, in the very least, at the possibilities and limitations. Our aim in this regard is to perform a feasibility study which will serve as input to future experiments.

We propose to use CLAS to investigate the $^3He(\gamma_t, V)^3He$, $^3He(\gamma_t, V)p(pn)_{sp}$, and $^3He(\gamma_t, Vp)(pn)_{sp}$ reactions, where $V = \rho^0$, $\omega$, or $\phi$ mesons, by detecting the hadronic decay modes indicated in Table 2. These modes were selected over the leptonic ones mainly because of their favorable branching ratios. It is clear that each reaction channel and each vector meson probe different aspects of medium modifications. Fortunately, the data for all these will be accumulated simultaneously in CLAS. The choices of $^3He$ as the nuclear target and 320-1520 MeV tagged photon energy contribute to the suppression of competing channels, including those which involve final state interactions of the decay hadrons. The key features of our physics methodology and motivation are expanded upon in the remainder of this section.

## 2.1 Vector Meson Production in the Subthreshold Region

The general physics topic of our proposal is similar to that of proposal E94-002 [38], however, *the subthreshold emphasis in this proposal is unique.* A detailed comparison of the two methods is outlined in the Appendix.

The diagrams that contribute to the vector meson production processes of interest to this proposal are shown in Fig. 3. The interaction vertex can be driven by the exchange of a pomeron, pion or vector meson. The exact mechanism, which depends on the four-momentum transfer, is not relevant to the investigation of this proposal; rather, only the kinematics of the reaction and the final state are of interest here,

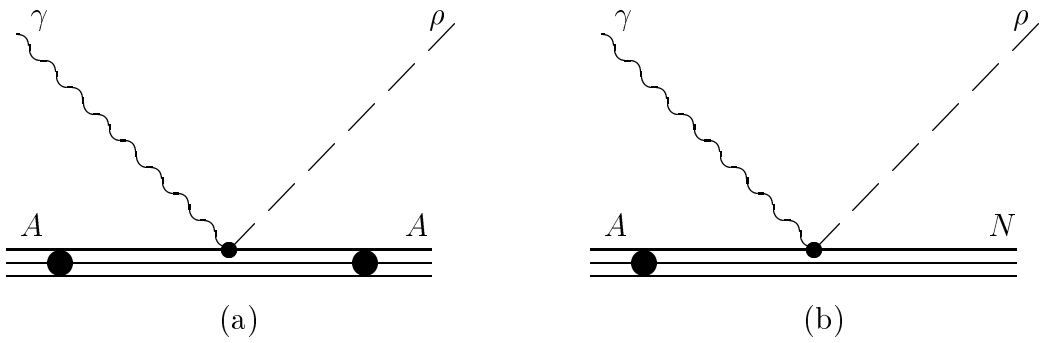


Figure 3: Diagrams contributing to the $\rho^o$ meson channel: (a) and (b) refer to the exclusive and breakup channels in the text, respectively, and contribute in the subthreshold region.

since the physics of vector meson medium modifications alone already define the scientific motivation of this proposal.

Above the threshold of vector meson photoproduction off a proton, at a nominal (mean) photon energy $E_\gamma = 1083$ MeV, the single nucleon amplitudes contribute coherently to the total vector meson production cross sections on nuclei, and as a result yield large cross sections. This was verified by $\rho^0$ production on nuclei at photon energies in the 2.6-6.8 GeV region [39]. However, in that energy region, where the momentum transfer to the struck nucleon is very small, $\rho^0$ mass modifications could not have been observed for two reasons: *first*, as $t \to 0$ in coherent (diffractive) $\rho^0$ production, the $\rho^0$-mesons are produced essentially outside the nucleus and only a fraction of them is expected to penetrate its interior region; *second*, among the ones that do penetrate, only a very small fraction will decay within the nuclear volume due to the $\gamma\beta c\tau$ factor. The latter argument is even more compelling for the $\omega$ and $\phi$ mesons, which have $c\tau$ factors of 24 fm and 45 fm, respectively. This effect is clearly illustrated in Table 3, for 5 GeV photons impinging on a $^3He$ nucleus as compared to the 1 GeV case. *Clearly, any attempt to produce vector mesons off nuclei at photon energies significantly above threshold, greatly decreases the sensitivity to medium modification effects.*

On the other hand, below the photoproduction threshold on a free nucleon, termed the **subthreshold region**, we essentially "force" the interaction vertex to occur within the nuclear volume, thus enhancing the probability of medium modifications. In this situation, the vector meson can be brought on-shell mainly in one of two ways:

1. By employing a small momentum transfer in the reaction, one probes primarily the low region of the Fermi-momentum distribution of the participating nucleon. This process is mainly associated with a bound $^3He$ nucleus in the

Table 3: Fraction of $\rho^0$ , $\omega$ and $\phi$ decays inside each nucleus, $f = (1 - e^{-\frac{R_A}{\gamma c\tau}})$.

| $E_\gamma$ | Target | $R_A$ $[fm]$ | $\gamma_{\rho,\omega}$ | $\gamma_\rho c\tau[fm]$ | $f_\rho$ (%) | $f_\omega$ (%) | $f_\phi^\dagger$ (%) |
|---|---|---|---|---|---|---|---|
| 5 $GeV$ | $^3He$ | 1.7 | 6.51 | 8.46 | 18 | 1.1 | 0.8 |
| 1 $GeV$ | $^3He$ | 1.7 | 1.23 | 1.60 | 66 | 5.6 | 3.5 |
| 1 $GeV$ | $^4He$ | 1.9 | 1.24 | 1.61 | 70 | 6.2 | 3.7 |
| 1 $GeV$ | $^{12}C$ | 2.74 | 1.29 | 1.68 | 80 | 8.5 | 5.1 |
| 1 $GeV$ | $^{208}Pb$ | 7.11 | 1.29 | 1.68 | 99 | 21 | 12.5 |
| † $E_\gamma$ is 1.2 GeV for the $\phi$ meson. | | | | | | | |

final state, as shown in Fig. 3(a). We term this as the **exclusive** channel. As the momentum transfer increases in the subthreshold region, the exclusive cross section decreases rapidly, falling with the $^3He$ elastic form factor.

There are two physics reasons in pursuing the exclusive channel: First, it naturally suppresses background processes associated with the emission of nucleons. Second, at higher photon energies it can lead to information on mean-field-induced modifications on $\rho^0$-mesons, which are produced coherently and decay within the nucleus.

2. By requiring a large four-momentum transfer in the reaction, compared to the average single (bound) nucleon's Fermi four-momentum, the region of large momentum components in the single nucleon wavefunction is probed. This process is represented diagramatically in Fig. 3(b) and it results, of course, in small cross sections, compared to the total $\rho^0$ cross section *above threshold*. Nevertheless, it dominates the cross section in the subthreshold regime and corresponds to a short-range $\gamma - N$ interaction. We refer to this reaction as the **breakup** channel and medium modifications may depend on the field of the interacting nucleon, due to the short-range nature of the interaction.

An additional and important benefit of subthreshold production is connected to the low photon energy employed. This involves a small Lorentz boost from the center-of-mass to the lab frame and, thus, vector mesons emerge with small velocities relative to the participating nucleon (nucleus), which results in an increased probability of the vector meson decaying *within* the nucleonic (or nuclear) field. This is dramatically illustrated in Fig. 4. Furthermore, the small kinetic energies of the produced $\rho^0$ and $\omega$ will allow the investigation of possible bound states in $^3He$, which can take place only at threshold or subthreshold energy regimes. Finally, the low Lorentz boost of the dipion center-of-mass in the laboratory frame preserves the large opening angle between the two pions, a correlation *unique* to the $\rho^0 \to \pi^+\pi^-$ decay among all other $\pi^+\pi^-$ producing reactions at these photon energies. This results in a critically effective selection criterion for suppressing backgrounds, while

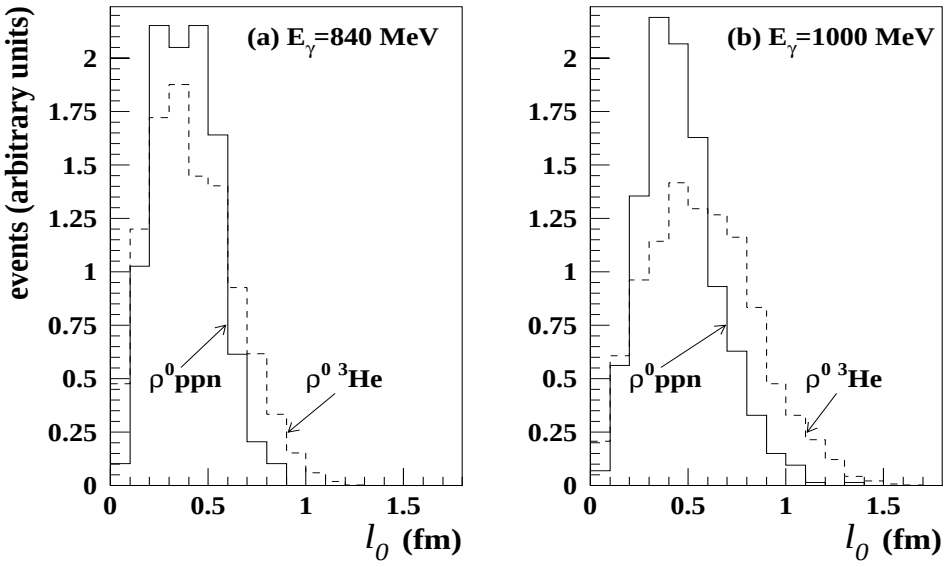


Figure 4: Simulated mean decay length $l_0$ distribution, of the $\rho^0 \to \pi^+\pi^-$ decay, is indicative of the distances probed for vector meson modifications in the TAGX experiment. The $l_0$ spectra are illustrated for (a) $E_\gamma$ = 840 MeV and (b) $E_\gamma$ = 1000 MeV. The histograms are for MC generated events accepted by the spectrometer in the $^3He(\gamma_t, \rho^0)p(pn)_{sp}$ (solid curves) and $^3He(\gamma_t, \rho^0)^3He$ (dashed curves) reactions, arbitrarily normalized. The mean decay length is for the former reaction in the rest frame of the participating proton (the two remaining nucleons being spectators), and for the latter in the rest frame of the $^3He$ nucleus. In either case, the $\rho^0 \to \pi^+\pi^-$ decay occurs predominantly within the hadronic volume of either the nucleon or the $^3He$ nucleus.

leaving the $\rho^0$ events in the data sample largely unaffected, as will be shown in greater detail in Section 4.2.1.

Even at subthreshold energies, however, a "natural" mass $\rho^0$ can be still be produced on $^3He$ , associated with either diagrams 3(a) or (b). At $E_\gamma$ = 870 MeV, for example, only half of the natural $\rho^0$ resonance can be populated in the invariant mass distribution, which means that this $\rho^0$ production process is suppressed due to phase space restrictions. Such production would amount to a "trivial" kinematical mass shift and will be unfolded in the analysis.

*In short, in our proposed experiment we aim to selectively examine regions of phase space where diagrams 3(a) and 3(b) are alternatively enhanced/suppressed, as they may probe nuclear versus nucleonic field modifications, respectively.* Both channels will be presented in further detail, following the discussion on the target nucleus.

## 2.2 The Choice of Nuclear Target

In principle, one desires as massive a target as possible (high $\rho_{nuc}$ and large charge distribution radius) in order to amplify the experimental nuclear medium modification signatures. However, for the $\rho^0 \rightarrow \pi^+\pi^-$ decay channel, this leads to the potential complication of final state interactions (FSI) of the decay pions via $\pi$-N scattering. Fortunately, in subthreshold production, where the vector meson is produced essentially at rest, the fraction of in-medium decays is high enough for light nuclei that a heavy nuclear target does not provide much of an advantage, as is evident in Table 3 and Fig. 4. This point is also reflected in the expected mass modification of the $\rho^0$ in a finite nuclear density distribution as calculated in the work of Saito et al. [40]. In this reference, unlike all other calculations which involve infinite nuclear matter, the experimentally parameterized charge density distributions for $^3He$, $^4He$, and $^{12}C$ were used. The values of $\delta m_{\rho^0}$ were calculated to be 40, 80, and 50 MeV/c$^2$, respectively, and the highest value reflects only the higher core density of $^4He$. Thus, for subthreshold $\rho^0$ production, a light nucleus coupled with the prolific branching ratio of the hadronic decay $\rho^0 \rightarrow \pi^+\pi^-$ has all the advantages.

There is an additional and practical reason why $^3He$ is the ideal *first* nuclear target for the study of the modifications of vector mesons: the scientific motivation of E93-044 [41] is centered on the investigation of all photoreaction channels, except subthreshold vector meson production. In essence, the foreground reactions of E93-044 are the background channels for this proposal. Such an ideal symbiosis of experiments is only achievable with the CLAS spectrometer in Hall B.

## 2.3 The Exclusive $^3He(\gamma_t, V)^3He$ Channel

Here the aim is to isolate diagram 3(a), which constitutes approximately 10% of the $\rho^0$ production cross section at typical subthreshold energies. This is accomplished by imposing selection criteria on the missing mass spectra (see Section 5), which allow access to regions of phase space where the small relative velocity between $V$ and $^3He$ maximizes the probability of the meson decaying within the nuclear density distribution, as shown in Fig. 4. An additional advantage is the natural suppression of the most prominent sources of $\pi^+\pi^-$ background, which involve the emission of energetic nucleons, thus resulting in cleaner $\rho^0 \rightarrow \pi^+\pi^-$ signatures in the data.

The TAGX experiments [32, 33] spurred specific theoretical calculations, based on the $QMC$ model of Saito, Tsushima and Thomas [40, 42]. The results of the calculation for $^3He$ were consistent with $\delta m_{\rho^0} = 40$ MeV/c$^2$, which is much smaller than the extracted values from the TAGX experiments. Given the mean field density of $^3He$, the calculation in [40] predicts a mass modification of about 8%, whereas the data support a number closer to 17%. This discrepancy is significant and must be pursued further with CLAS.

### 2.4 $^3He(\gamma_t, V)p(pn)_{sp}$, $^3He(\gamma_t, Vp)(pn)_{sp}$ Breakup Reactions

As reported in references [32, 33, 34], the breakup reaction in diagram 3(b) dominates the total $\rho^0$ photoproduction cross section in the subthreshold region. The relative momentum between the $\rho^0$ and the struck nucleon is such that the majority of the $\rho^0$ particles will decay within the hadronic field of the nucleon [43]. At $E_\gamma$ = 840 MeV, approximately 70% of the produced $\rho^0$ mesons decay within 0.5 fm from the production vertex, as shown in Fig. 4. Therefore, for such regions of phase space, new aspects of $\rho^0 - N$ interactions can be probed.

These new possibilities seem to be supported by the findings of reference [8], in which energy densities of 1 GeV/fm$^3$ result in chiral symmetry restoration. Such densities are manifested within the nucleonic domain. It turns out that, at $\rho^0$ -N relative coordinates of 0.5 fm or less, the nucleon's hadron matter density is high enough to exceed $\rho_{nuc}$, and thus induce a mass modification that cannot be realized in the context of the nuclear mean field. If this is indeed the case, in subthreshold vector meson production, the mass modification should be nearly independent of mass number. This **nucleonic effect** has not been considered in any of the theoretical calculations, and has been reported for the first time in reference [32].

For the $\omega$ and $\phi$ , due to their longer $c\tau$, it is even more critical to be selective in terms of phase space, in order to probe low $V - N$ relative velocities. In these regions, we not only expect to maximize the mass modification, but to also increase the ratio of modified to unmodified $V$-mesons, as well.

## 3 The Experiment

Here, we outline the most important experimental requirements and considerations necessary to perform the experiment. Certain quantities in this section have been determined by Monte Carlo simulations (Sections 4 and 5) and have also been cross checked against the TAGX experimental results.

### 3.1 Experimental Parameters

The basic requirements for the experiment are listed in Table 4. This information was employed in the Monte Carlo simulations and count rate estimates, discussed later in this section. A matter of importance is that the tagger should be operated using the entire tagging range from 20% to 95% of the endpoint energy. This will allow us to probe deep into the subthreshold region and will permit access to regions where background reactions dominate, providing information that will be used in the deconvolution of the data. It will also lead to coherent production of the $\rho^0$ and $\omega$, which will be used as a check of the experimental consistency and resolution. The coherent $\omega$ signature will also assure us that the $\phi$ can also be identified subthreshold, since coherent $\phi$ production is not accessible in this experiment.

Table 4: Proposed Experimental Parameters.

| | |
|---|---|
| Electron Energy | 1.6 GeV |
| Photon Energy Range | 0.32 - 1.52 GeV (0.20-0.95$E_o$) |
| Beam current | 8 nA |
| Number of tagged photons | $10^7\gamma/s$ |
| E93-044 Target density | 1.0 g/cm$^2$ |
| E93-044 Target material | liquid $^3He$ |

## 3.2 Trigger

The optimum condition for this experiment requires two charged particles in the trigger, and an open neutral trigger. This will ensure that events of the types $\pi^+\pi^-$, $\pi^+\pi^-\pi^0$ and $\pi^+\pi^-p$ will be accepted, as well as those where additional nucleons/pions emerge. The sorting of the different reaction channels will be performed off-line. A detailed trigger simulation along the lines of that performed for E93-031 [45] has been performed and continuous refinements are being incorporated.

The optimal trigger as such appears rather restrictive. However, as verified in the "leptonic-background free" conditions encountered in the *g6* running period, the limit on the photon flux, and thus the beam time required, is defined by the accidental rates. From our MC simulations and accidental rates, we believe that the two-charged-particle trigger results in the most efficient use of beam time needed to accomplish the scientific goals of the experiment.

## 3.3 Optimal Magnetic Field and Tagger Energy

The events were generated with codes based on the GENBOD package. For each reaction considered, 250,000 events were generated, taking into account the Fermi distribution for single nucleons in $^3He$. These events, in turn, were fed into the CLAS detector simulation package, GSIM. The resulting pristine output file was then analyzed with the Hall B analysis package, RECSIS, the final result being an ntuple file for each generator. We note that no trigger requirements were imposed in the RECSIS analysis; this was handled entirely within the subsequent ntuple analysis.

The objective of these studies is to optimize the acceptance for the foreground reactions by looking at its dependence on the magnetic field of the torus and the tagged photon energy region. In general, with positive particles bending outward, the geometrical acceptance for protons is not drastically affected by choice of field strength. However, this is **not** necessarily the case for pions, where the $\pi^+$ are bent outward and the $\pi^-$ inward and *away* from the detectors.

We define the acceptance in the usual way:

$$\epsilon = \frac{N_{\rm acc}}{N_{\rm gen}} \tag{5}$$

where $N_{\rm gen}$ is the total number of events generated and $N_{\rm acc}$ represents the numbers of events accepted after passing all cuts.

We simulated $\epsilon$ at $E_\gamma = 0.8$, 1.0 and 1.2 GeV, and at B-field values of +0.25, +0.50 and +0.90 times the nominal field strength for the ${}^3He(\gamma_t, \rho^0)p(pn)_{sp}$ reaction, and for a shifted $\rho^0$ mass of 600 MeV/c$^2$. The results are shown in Table 5 and plotted in Fig. 5. The columns are labelled according to the particles detected in CLAS. The final column is the total geometrical acceptance for the combined $\pi^+\pi^-$, $\pi^+\pi^- p$ and $\pi^+\pi^- p(p)$ events.

Table 5: Magnetic field acceptance studies for $m^*_{\rho^0} = 600$ MeV/c$^2$.

| ${}^3He(\gamma_t, \rho^0)p(pn)_{sp}$ | | | | |
|---|---|---|---|---|
| B/B$_\circ$ | $\epsilon_{\pi^+\pi^-}$ | $\epsilon_{\pi^+\pi^- p}$ | $\epsilon_{\pi^+\pi^- p(p)}$ | Total $\epsilon$ $(\Sigma\rho^0)$ |
| | $E_\gamma = 0.8$ GeV | | | |
| +0.25 | 12.8% | 8.8% | 0.7% | 22.3% |
| +0.50 | 9.4% | 6.4% | 0.4% | 16.2% |
| +0.90 | 4.2% | 2.2% | 0.2% | 6.6% |
| | $E_\gamma = 1.0$ GeV | | | |
| +0.25 | 8.5% | 11.0% | 3.0% | 22.5% |
| +0.50 | 6.5% | 7.9% | 2.0% | 16.4% |
| +0.90 | 3.1% | 3.1% | 0.7% | 6.9% |
| | $E_\gamma = 1.2$ GeV | | | |
| +0.25 | 5.8% | 11.3% | 6.0% | 23.1% |
| +0.50 | 4.2% | 7.8% | 3.4% | 15.4% |
| +0.90 | 2.1% | 3.1% | 1.3% | 6.5% |

From this table, we note several important features. The first is that the acceptance of the $\pi^+\pi^-$ channel drops by a factor of two from 0.8 GeV to 1.2 GeV, whereas that for the $\pi^+\pi^- p$ channel increases by 30% over this region and the $\pi^+\pi^- p(p)$ also increases, but by a factor of eight. These features are understood by noting that events that are lost from the $\pi^+\pi^-$ sample end up in the $\pi^+\pi^- p$ events because the participating proton gains enough energy to make it into the CLAS acceptance. A similar exchange occurs between the $\pi^+\pi^- p$ and $\pi^+\pi^- p(p)$ subsets. The combined gain and loss of events in the $\pi^+\pi^- p$ channel, due to its two neighbor channels, results in an overall 30% gain.

The second – and most important – point is that the acceptance for both $\pi^+\pi^-$ and $\pi^+\pi^- p$ drops dramatically as a function of B/B$_\circ$: we lose a factor of three

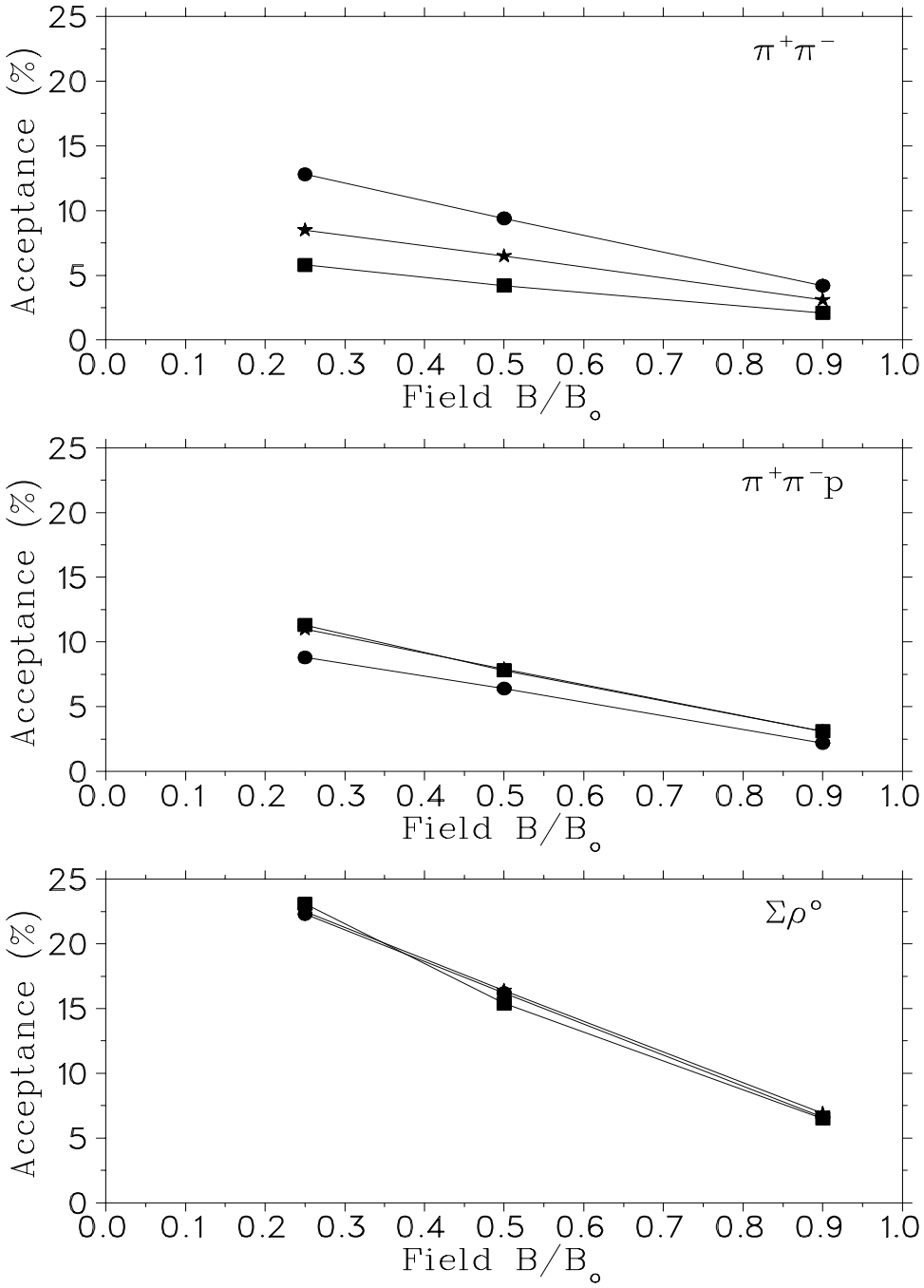


Figure 5: Simulated CLAS acceptance for the $^3He(\gamma_t, \rho^0)p(pn)_{sp}$ reaction as a function of magnetic field. The circles, stars and squares represent $E_\gamma$ at 0.8, 1.0 and 1.2 GeV. The top and middle panels are for the $\pi^+\pi^-$ and $\pi^+\pi^-p$ channels, respectively, whereas the bottom panel represents the total efficiency from Table 5.

in acceptance from +0.25 to +0.90. Moreover, this loss is not uniform: it affects different regions of phase space in a different manner, which is detrimental to this experiment, especially for the $\omega$ and $\phi$ analyses. As will be shown in Sections 4 and 5, detecting one or both of the final state protons is a significant advantage in suppressing the background processes. Finally, we have examined the affect of the field on the energy resolution and we have determined that it is rather insignificant.

*We conclude that, the optimal field for the $\rho^0$ channel is at* $\mathrm{B/B_\circ} = +0.25$. *The same will hold true for the $\omega$, due to the extra $\pi^0$ in the decay which participates in the sharing of the available kinetic energy. Any significant mass reduction, either due to in-flight or bound state mechanisms, will further reduce the mean pion momenta, thus making the low-field setting even more critical for acceptance maximization. The low-field constraint is compatible with only a fraction of the beam time hours currently scheduled for the g3 beam period.*

## 3.4 Reaction-Specific Geometrical Acceptance Studies

In Table 6, we list the acceptances of the foreground and background reactions, as described in Section 4.1, for the $\pi^+\pi^-$ events, the $\pi^+\pi^- p$ events, and the sum of the two. As is apparent in this table, the acceptance for the foreground channels is quite satisfactory. As a further check of our MC analysis procedure, the $\omega \to \pi^+\pi^-\pi^0$ and the breakup $\rho^0$ production leading to the $\pi^+\pi^- p$ channel were also simulated with the FASTMC code [46], and the results were in agreement with those shown in Table 6.

Table 6: Geometrical Acceptance of CLAS for Channels Described in Section 4.1, for $\mathrm{B/B_\circ}$=+0.25, $E_\gamma$ = 1.0 GeV and $m^*_{\rho^o}$ = 600 MeV/c$^2$.

| Reaction | $\epsilon_{\pi^+\pi^-}$ | $\epsilon_{\pi^+\pi^- p}$ | Sum |
|---|---|---|---|
| Exclusive $\rho^0$ production | 18% | 0% | 18% |
| Breakup $\rho^0$ production | 9% | 11% | 20% |
| Exclusive $\omega$ Production | 5% | 0% | 5% |
| Breakup $\omega$ production | 4% | 3% | 7% |
| Single $\Delta$ production | 9% | 9% | 18% |
| Quasifree $N^*$ production $^{(*)}$ | 5-8% | 3-8% | 8-16% |
| Double $\Delta$ production | 6% | 11% | 17% |
| Incoherent $\pi^+\pi^-\pi^0$ (Exclusive) | 14% | 0% | 14% |
| Incoherent $\pi^+\pi^-\pi^0$ (Breakup) | 3% | 2% | 5% |
| $^{(*)}$ indicates different resonances considered | | | |

### 3.5 Precision Expected

The MC fitting procedure assumes constant matrix elements within each tagged photon energy bin. In this experiment, we plan to use 20 MeV bins. This fine photon energy bin will allow a very reliable fitting of the simulations of different processes, both because the matrix elements vary very little in such small increments, and because the larger number of data allow a higher fitting confidence in the overall MC fitting algorithms. Furthermore, an accurate determination of $m^*_{\rho^o}$ from the $l = 1$ angular distribution analysis (see Fig. 2) can be obtained by binning the invariant mass in 50 MeV/c$^2$ (or even finer) intervals, *for each of the 20 MeV energy bins around the critical subthreshold regions for nucleonic and nuclear sources of modification.* This will allow for a definitive interpretation of the collected data. With this binning in mind, a 5% (high confidence) measurement in each bin may be achieved by requiring $N_{\rho^0} = 10{,}000$ $\rho^0$ events, see Sections 4 and 5.

The precision of the proposed experiment will far exceed all previous results, as shown in Fig. 6. In this figure, the results from the two TAGX experiments on $^3He$ are shown [32, 33], and are compared to a simple model calculation which assumes production on a nucleon in $^3He$ by folding the nucleon density distribution, the single nucleon Fermi momentum distribution in $^3He$, and the phase space available due to the beam energy and TAGX acceptance [24]. As a comparison, the expected CLAS results are also shown, as if they follow the simple model curve.

## 4 Background Suppression Methodology

Whereas the hadronic decay $\rho^0 \rightarrow \pi^+\pi^-$ has the advantage of a large branching ratio, the strength of "physics background" processes, which also contribute to $\pi^+\pi^-$ production, is significant. Thus, the issue of background suppression, *in a way that will not affect the spectral shape of the* $\rho^0$, is of paramount importance to the success of the project. In this section, we present the philosophy behind the background suppression, and then apply it to the analysis in Section 5.

### 4.1 Extraction of the V mass from the data

At present, we propose to extract the modified vector meson mass from the CLAS data in a manner similar to our already published TAGX analyses [32, 33, 34]. Our analysis method is under constant refinement and improvements have already been incorporated in the CLAS analysis. For the sake of brevity, the following discussion will consider V = $\rho^0$ only.

As will be explained in Section 5, we plan to analyze two-, three-, and four-track CLAS data, including $\pi^+\pi^-$, $\pi^+\pi^-p$ and $\pi^+\pi^-p(p)$ events, in addition to events containing a detected $\pi^o$. This is because the different physics processes, which contribute significantly to $\pi^+\pi^-$ photoproduction in this energy region, can also result in the emission of one or more energetic nucleons. *The extraction of*

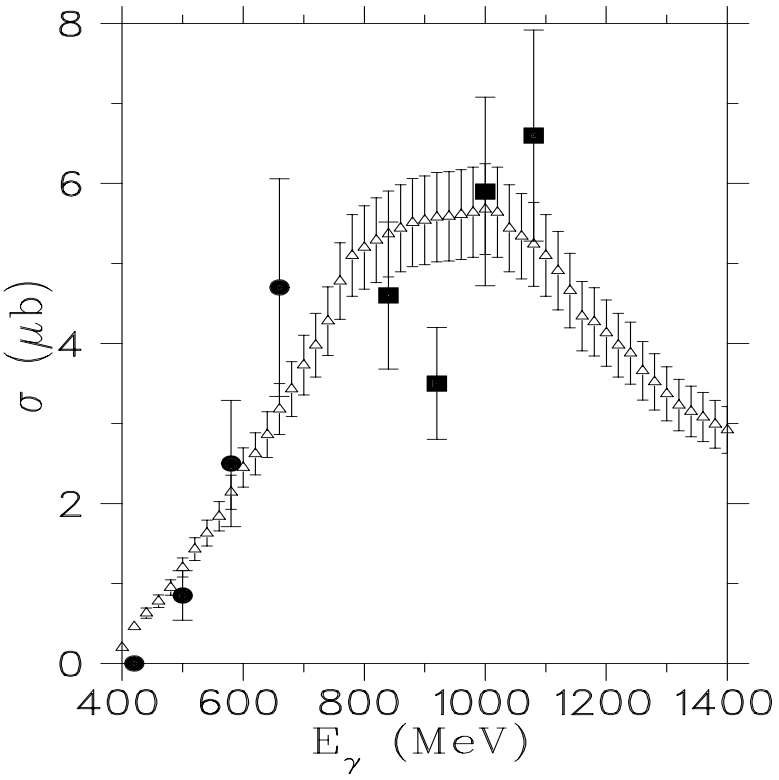


Figure 6: The cross section for the ${}^3He(\gamma_t, \rho^0)p(pn)_{sp}$ channel, assuming a mass of 600 MeV/c$^2$ for the shifted $\rho^0$ meson. Filled boxes and circles represent the numbers extracted with the MC fitting technique from references [32] and [33], respectively. The open triangles depict the expected CLAS results from the ${}^3He(\gamma_t, Vp)(pn)_{sp}$ channel, assuming that they follow the simple model calculation, which has been arbitrarily normalized to the data distribution. A 10% overall systematic error for the CLAS results has been assumed in this simulation.

*these multitrack data, from the large CLAS acceptance, together with the greatly improved statistical precision, will provide a striking advance over any other previous experiment.*

In the remainder of this section, we will present the physics background processes, as well as specific cuts which suppress their contributions to the data. Briefly, the physics background processes that we have to consider here are production reactions and FSI:

### 4.1.1 Background from Production Reactions

- ${}^3He(\gamma, \Delta\pi)$ on a nucleon, followed by $\Delta\pi \rightarrow \pi^+\pi^- N$ (the two other nucleons are spectators). This is the dominant $\pi\pi$ production mechanism in the 1 GeV

region [47]. As this process usually results in the emission of an energetic nucleon, it will contribute to both the two- and three-track event samples. This process is greatly suppressed in the exclusive $\pi^+\pi^-$ channel.

- Quasifree $N^*$ production, ${}^3He(\gamma, N^*\pi)$ or ${}^3He(\gamma, N^*)$ on a nucleon, which decays via $N^* \to \pi N$ and $N^* \to \Delta\pi \to \pi\pi N$, respectively. Here $N^*$ includes the Roper, the $N^*_{1520}$, and other higher nucleonic resonances, as appropriate. These processes gain importance as the incident photon energy is raised to the 1-1.5 GeV region, otherwise they are similar to the quasifree $\Delta\pi$ channel.

- ${}^3He(\gamma, \Delta\Delta)$ on a nucleon pair, followed by $\Delta\Delta \to \pi^+\pi^- NN$. This reaction has been measured on both ${}^2H$ [48, 49] and ${}^3He$ [50] targets, and is an important process at 1 GeV. It does not contribute to the exclusive $\pi^+\pi^-$ channel.

- Incoherent $\pi^+\pi^-\pi^0$ production. At 1 GeV, this channel is fairly weak, but it contributes to the high missing momentum region. The neutrals capability of CLAS should aid in the understanding of this portion of the data set, and will be especially helpful in the $\omega$ and $\phi$ analyses.

### 4.1.2 Final State Interactions

One of the prime motivating factors in the pursuit of the leptonic $V \to e^+e^-$ decay channel is the lack of FSI compared to the hadronic channel. Indeed, final state interactions, of the form $\pi N \to \pi' N'$, can occur between the pions produced from $\rho^0$ decay and one of the nucleons, possibly mimicking the signature of a medium modified $\rho^0$ mass and leading to erroneous conclusions. Although such effects are expected to be minimal for ${}^3He$ – and TAGX has confirmed this – they will be modelled and included in the fitting procedure. The physics reasons for such minimal influence are:

1. One of the dominant FSI processes in nuclei is pion absorption, $\pi^+ NN \to NN$. This results in the removal of the event from our trigger and does not represent a problem, as our method of $m^*_{\rho^o}$ extraction is independent of $\sigma_{\rho^0}$.

2. In the ${}^3He(\gamma_t, V){}^3He$ reaction, the forward peaked $\pi N \to \pi' N'$ scattering will not distort any extracted $\rho^0$ spectra, as it involves very small momentum transfer. Larger momentum transfer scattering is suppressed by DWIA arguments, since the ${}^3He$ must remain intact. Inelastic $\pi N$ scattering (pion production) is discriminated against by missing mass cuts.

3. In the ${}^3He(\gamma_t, Vp)(pn)_{sp}$ reaction, if the four-momentum is large enough to change the extracted $m_{\rho^o}$, the FSI and $\rho^0 \to \pi^+\pi^-$ channels can be separated based on their different kinematical signatures which result in the population of different regions of phase space. Indeed, this has been verified in the TAGX analysis of the ${}^3He(\gamma_t, V)p(pn)_{sp}$ reaction, which is less restrictive, and, in principle, more difficult to analyze than the ${}^3He(\gamma_t, Vp)(pn)_{sp}$ channel.

4. Finally, if $\pi N \to \pi' N'$ events survive all cuts and if the momentum transfer to the struck nucleon is large enough to affect $m_{\pi^+\pi^-}$, the $p$-wave signature of the dipion system will also be lost. **A clean *p*-wave signature is final proof of minimal FSI**.

## 4.2 Global Background Suppression Techniques

Among the background production reactions above, the most prominent in terms of cross sections are the $\Delta\pi$ (combined with the $N^*\pi$ and $N^*$ reactions), and the $\Delta\Delta$ reactions. The $\Delta\pi$, $N^*\pi$ and $N^*$ production reactions have phase space distributions so similar to each other that they can all be represented effectively by the $\Delta\pi$ kinematics. The specific reactions simulated, taking all angular momentum quantum numbers and isospin projections into consideration, are: $\Delta^{++}\pi^-$ and $\Delta^{++}\Delta^-$. In this context then, when we refer to the $\Delta\pi$ cross section, we include the $N^*$ and $N^*\pi$ contributions. A comparison of these cross sections to that for the modified $\rho^0$ ($m^*_{\rho^0} \approx 600$ MeV/c$^2$) for $E_\gamma \approx 800$ MeV, establishes the relative importance to the total $\pi^+\pi^-$ cross section **per nucleon (or pair of nucleons)**:

- $\sigma_{\Delta\pi} \approx 36\mu b$
- $\sigma_{\Delta\Delta} \approx 37\mu b$
- $\sigma_{\rho^0} \approx 4\mu b$

At first glance, it appears that the extraction of the $\rho^0 \to \pi^+\pi^-$ reaction, with any reasonable confidence, will be very problematic. However, among all these $\pi^+\pi^-$ producing processes, only the $\rho^0 \to \pi^+\pi^-$ reaction produces two *correlated* pions from the same physics vertex. Thus, the $\pi^+\pi^-$ acceptances ($\epsilon$) of any detector will also vary depending on the physics process, as shown in Table 6. For example, from the TAGX analysis we have:

- $\epsilon_{\Delta\pi} \approx 0.009$
- $\epsilon_{\Delta\Delta} \approx 0.006$
- $\epsilon_{\rho^0} \approx 0.04$

The yields ($Y$), which are the products of cross sections and acceptances for the TAGX experiments were:

- $Y_{\Delta\pi} \approx 324$ *a.u.*
- $Y_{\Delta\Delta} \approx 222$ *a.u.*
- $Y_{\rho^0} \approx 160$ *a.u.*

As a result of the acceptances, the measured yields from the $\rho^0 \to \pi^+\pi^-$ reaction are reasonable fractions of the total $\pi^+\pi^-$ yields. Furthermore, and just as importantly, **the phase space distributions for the various observables used in the analysis are not uniformly distributed**. In certain regions of phase space, the fraction of pion events from the $\rho^0 \to \pi^+\pi^-$ is higher than those of the main competing processes [32, 33, 34].

The are two main reasons why the TAGX acceptance for the $\rho^0 \to \pi^+\pi^-$ reaction is higher than that of the competing background processeses: (a) the requirement that the $\pi^+$ and $\pi^-$ are detected on opposite sides of the photon beam with large relative azimuthal opening angles, probes regions of phase space favorable to $\rho^0$ production; (b) the higher pion energies (on the average) resulting from the $\rho^0 \to \pi^+\pi^-$ decay, compared to all other two step processes, result in lower effective thresholds for the foreground reaction. This "built-in" background suppression by hardware design was a crucial factor in the eventual extraction of the $\rho^0$ signature from the total data in TAGX. CLAS, on the other hand, has equally large acceptances for foreground and background reactions, as shown in Table 6. This dictates the necessity of different and additional suppression techniques for CLAS data analysis, a fact which, at the same time, reduces the extrapolations necessary for the final extraction of cross sections.

**Thus, background suppression is simply equivalent to reducing the kinematical acceptance of CLAS for specific background reactions. This is accomplished with additional data cuts by taking advantage of the specific kinematical signatures of various reactions and the intrinsic capabilities of CLAS**.

### 4.2.1 Opening Angle Correlation, $\theta_{\pi\pi}$

There is a global criterion which is very effective in suppressing non-$\rho^0$ background, because it is applied *in addition and independently* of all other cuts and is applicable to both $\pi^+\pi^-$, as well as $\pi^+\pi^-p$ events. It stems for the fact that from the $\rho^0 \to \pi^+\pi^-$ decay, the two pions emerge back-to-back in the center-of-mass of the $\rho^0$. The modest kinetic energies of the $\rho^0$, in the subthreshold regime, preserve this large opening angle in the tranformation to the laboratory frame. All other competing reactions emit the two pions with opening angles more or less randomly distributed in any frame of reference. This is shown in Fig. 7, which shows the opening angle distributions $\theta_{\pi\pi}$ for three processes: $\Delta\pi$, $\Delta\Delta$, and $\rho^0$.

It is clear from Fig. 7 that a cut with $\theta_{\pi\pi} \geq 100^o$ greatly reduces the background events, without significantly affecting the events from the $\rho^0$ decay. An optimum value for this cut, which maximizes the foreground-to-background, $\rho^0$ over non-$\rho^0$ event ratio $(F/B)$, has been determined to be for $120^o$. The effect of this cut is dramatic, as illustrated in Fig. 8, which consists of TAGX data on deuterium and carbon in a mixture of $^{12}C$ and $CD_2$ targets. **This is one of the most effective cuts available to suppress the $\Delta\pi$ process and it is equally effective for**

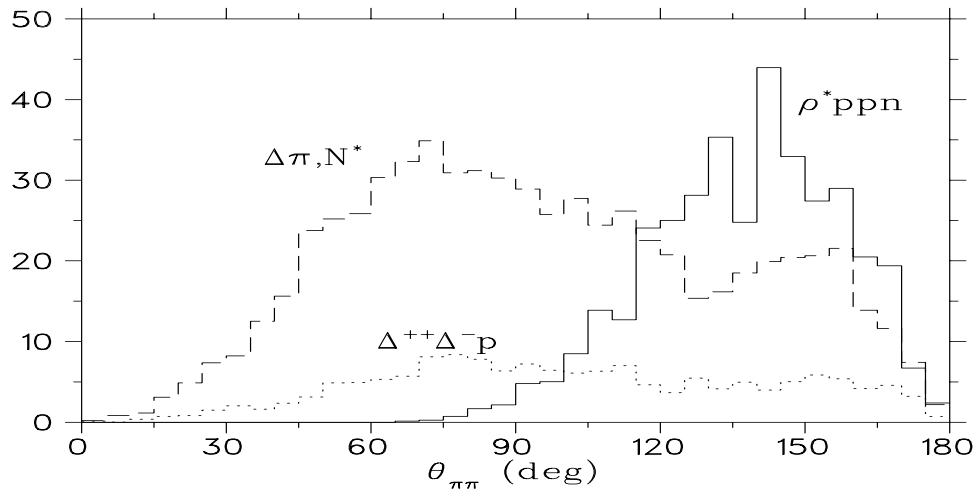


Figure 7: MC simulations showing the relative opening angle, $\theta_{\pi\pi}$, distributions for the $\rho^0$- (solid line), $\Delta\pi$- (dashed line) and $\Delta\Delta$-decays (dotted line) into two pions. The three reactions simulated are weighted by their cross sections and acceptances; the $\Delta\pi$ distribution includes, in addition, the estimated cross sections for the $N^*$ contributions not folded in the $\sigma_{\Delta\pi}$ in Section 4.2. The arrow, at $\theta_{\pi\pi} = 120^o$, indicates the opening angle cut applied to the analysis in Sections 5.1 and 5.2.

**all background contributions**.

A number of important conclusions can be drawn from Figs. 7 and 8.

### On Background Suppression

1. The $\theta_{\pi\pi} \geq 120^o$ cut, results in a suppression of the background in the 300-400 MeV/c$^2$ bin by a factor of approximately *five* (Fig. 8). The shape of the distribution has also changed between top and bottom panels, which is consistent with a greater suppression of the $\Delta\pi$-like background channels, which peak at $\cos\theta^*_{\pi^+} = 0$, rather than the corresponding ones for $\Delta\Delta$, incoherent, and $s$-wave $\pi^+\pi^-$ production reaction mechanisms, which exhibit flatter distributions in $\theta^*_{\pi^+}$. This cut does not distort the spectral shape of the $\rho^0$ mesons surviving the cut, and whatever small effect it may have, it is easily and reliably accounted for in the MC fits to follow.

2. In the invariant mass bin in Fig. 8(e), the opening angle requirement has dramatically reduced the number of events within the $\pm 0.5$ region, also by approximately a factor of *five* at $\cos\theta^*_{\pi^+} = 0$. However, the number of events at the $\pm 1$ general regions is affected very little, with an estimated loss of approximately 15%. This is consistent with Fig. 7 and with the back-to-back signature of two pions from $\rho^0 \to \pi^+\pi^-$ decay.

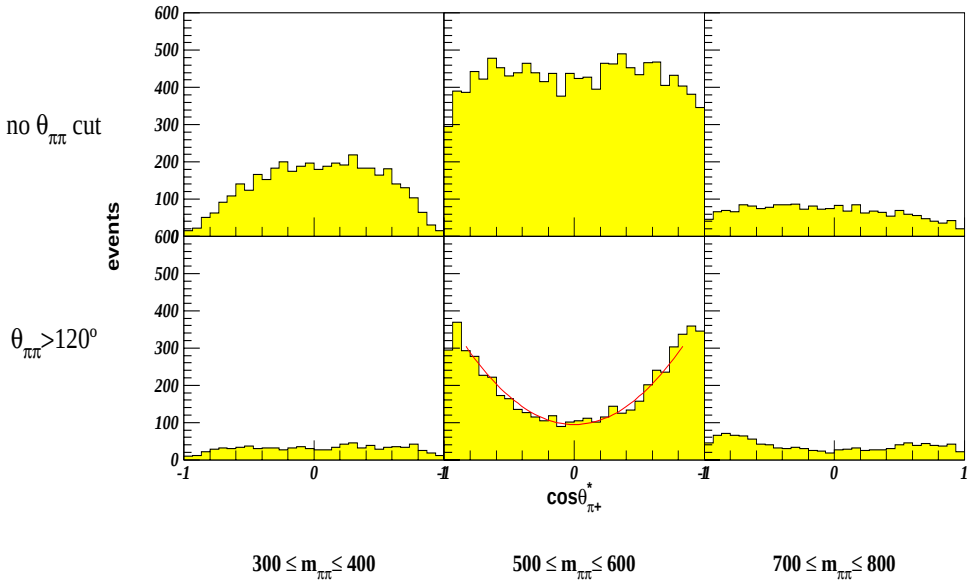


Figure 8: Selected invariant mass bins for data from the $^2H,^{12}C(\gamma,\pi^+\pi^-)X$ experiment obtained with TAGX. The top panels have no $\theta_{\pi\pi}$ cut, whereas the bottom panels have been subjected to a $\theta_{\pi\pi} \geq 120^o$ cut. The invariant mass bins for 400-500 and 600-700 MeV/c$^2$ also exhibit a $p$-wave signature, but it's neither as strong nor as symmetric as that in the 500-600 MeV/c$^2$ bin; they are not shown here for the sake of clarity.

3. The distribution in Fig. 8(e), also emphasizes the significant fraction of modified $\rho^0$ events in the data sample, even with only this assumption-free requirement, coupled to the acceptance bias of TAGX which favours the $\rho^0 \to \pi^+\pi^-$ reaction. In **this particular invariant mass bin**, $F/B \approx 2.5$.

### On The $J = 1$ Signature

1. Assuming that no $\rho^0$ strength is present in the 300-400 MeV/c$^2$ invariant mass bin in Fig. 8(a), it is clear that the background processes do not contribute to the vicinity of the $\pm 1$ regions of $\cos\theta^*_{\pi^+}$. As such, the distribution in panel (b) already indicates a sizable contribution from a new process (or processes), in addition to those in the lower invariant mass range. These additional processes are filling-in the extreme regions around the $\pm 1$ values.

2. **The relative $l = 1$ state of the two pions with respect to their center-of-mass is indicative of the $\rho^0 \to \pi^+\pi^-$ decay, and it cannot include another participating particle**. The $\Delta\pi$ production, for example, decays into a $\pi^+\pi^-$ pair, which still leaves a nucleon as participant in the reaction; angular momentum considerations can couple one pion to the nucleon in a

relative $l = 1$ state, but **cannot generate** a total angular momentum $J = 1$ correlation between the two pions, since they are generated at different vertices.

3. The symmetry of the distribution in the 500-600 MeV/c$^2$ bin in panel (e), is characteristic of a peak in the $\rho^0$ yield in this invariant mass range. In other words, it signifies a modified $\rho^0$ mass in the region $500 \leq m^*_{\rho^0} \leq 600$ MeV/c$^2$. A more precise value will be extracted after the completion of the analysis, which involves unfolding the phase space distribution and TAGX acceptance, in order to turn yields into spectral shapes.

4. Finally, the very weak $p$-wave signature observed in panel (f), is consistent with a weak production of natural mass $\rho^0$ mesons, a production which is severely suppressed in subthreshold energy regimes due to phase space restrictions.

### 4.2.2 The $p^*_T$ *vs* $\cos\theta^*_{\pi^+}$ Correlation

Since the $\rho^0 \to \pi^+\pi^-$ decay is the **only** single vertex decay into two pions present in the data sample, we can employ additional cuts, using only kinematical variables. A correlation often used in particle physics to isolate such type of decays, from those from two-step and uncorrelated competing processes, is that between the transverse momentum of one pion (with respect to the dipion plane), $p^*_T$, and $\cos\theta^*_{\pi^+}$, and shown in Fig. 9.

Following application of the global $\theta_{\pi\pi} \geq 120^o$ cut to suppress non-$\rho^0$ background and enhance the $p$-wave signature of the $\rho^0$, a cut can then be applied around the $\rho^0$ locus in Fig. 9(a) to eliminate a fraction of the two pions originating from the background processes. Such a cut still preserves a measure of the background within the locus encompasing the $\rho^0 \to \pi^+\pi^-$ decay events, by including the region $\cos\theta^*_{\pi^+} = 0$, where the $\rho^0 \to \pi^+\pi^-$ decay has zero population. This is now a flat background and does not affect the shape of the exclusively $\rho^0$ signatures, as has been shown in Fig. 8.

## 4.3 Conclusions on Background Suppression

In conclusion, Fig. 8 is the assumption-free, "smoking-gun" type of proof that the mass of the $\rho^0$ in-medium is modified by a significant amount and that the background suppression techniques followed are quite successful in extracting the $\rho^0$ signatures. The combination of the two "global" cuts in Section 4.2 has **reduced the acceptance of background by a factor of six**, while the acceptance of the $\rho^0$ foreground has been reduced only by $\approx 30\%$, averaged over all phase space. In selected regions of phase space, where the modified $\rho^0$ signatures manifest themselves, we show $F/B \geq 2.5$.

We are now ready to apply reaction-specific cuts to CLAS simulated events.

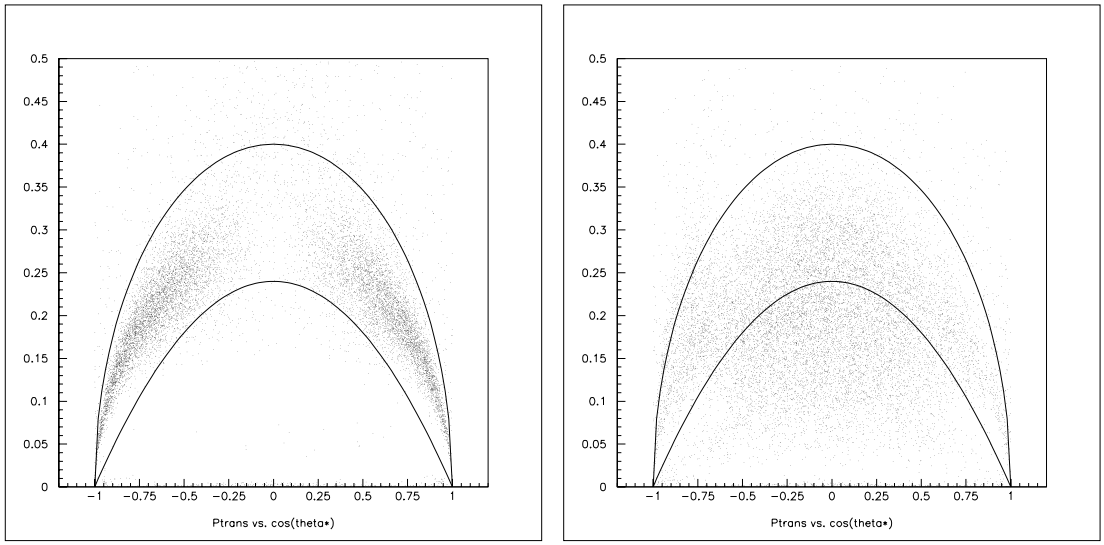


Figure 9: Correlation plot between the transverse momentum of one pion with respect to the dipion momentum plane, and the angle of that pion with respect to the dipion momentum in the lab frame ($p^*_T$ $vs$ $\cos\theta^*_{\pi^+}$) for: (a) the $\rho^0 \rightarrow \pi^+\pi^-$ decay ($m^*_{\rho^0}$=650 MeV/c$^2$); and (b) the $\Delta\pi$ reaction. The locus shown by the solid line indicates the area where a cut is placed to exclude events clearly outside the $\rho^0$ correlation area in the data sample. This figure is generated by the CLAS MC simulation package and has been confirmed against TAGX data.

# 5 Analysis of Events with CLAS

The analysis of CLAS data will be very similar in philosophy to the TAGX analysis [32, 33, 34]. The data will be ultimately deconvoluted with the aid of MC physics generators. These are purely phase-space driven, in the sense that the matrix element is taken as constant in each tagged-photon energy bin, and as such, **the conclusions are the least affected by amplitude interference among the various coupled background channels**. As with the TAGX analysis, the fitting procedure will be an *iterative and simultaneous fitting of several experimental observables*, with the data from each photon energy bin *treated completely independently of the others*. The very good statistics afforded in the proposed experiment will allow a fine binning of only 20 MeV, which increases the confidence and self-consistency in the fitting, since the constancy of the matrix elements is assured.

These experimental observables are:

- The dipion invariant mass $m_{\pi\pi}$.
- The missing mass $m_{miss}$.
- The opening angle between the two pions $\theta_{\pi\pi}$.

- The missing momentum $p_{miss}$.
- The emission angle of the $\pi\pi$ system $\theta_{IM}$.
- The cosine of the pion angle, $\theta^*_{\pi^+}$.

The fitting will also be carried out simultaneously in three missing mass regions for unselected (no cuts) and $\rho^0$ -enhanced (cuts imposed) data sets.

1. Focusing on the breakup channel of $^3He$.
2. Focusing on the exclusive ( $^3He$ ) region.
3. The final missing mass region is unrestricted.

Such a fit is not optimized just on the $\pi^+\pi^-$ invariant mass, as with the CERES analysis, but takes into account the distribution of the data over a wide range of experimental observables. This is intended to reduce the chance of a fortuitous fitting to the data, and the extraction of an erroneous modified $\rho^0$ invariant mass or width.

We separate the analysis package into two different sets, depending upon whether or not the associated proton is detected in the CLAS detector, in addition to the $\pi^+\pi^-$ events.

## 5.1 Analysis of $\pi^+\pi^-$ Events

The analysis of the $\pi^+\pi^-$ events (no proton detected) is the most limiting one, because the coplanarity capability of CLAS cannot be fully utilized to further suppress background. As an example of the effectiveness of the cuts from Sections 4.2.1 and 4.2.2, we have simulated three production channels: $\Delta\pi$, $\Delta\Delta$, and $\rho^0$, in accordance with the production cross sections from Section 4.2. The CLAS acceptances from MC simulations (Table 6) have been folded in the distributions of Fig. 10.

It is clear from this figure that the background suppression is quite satisfactory. The $F/B$ ratio in $p_{miss}$, $m_{\pi\pi}$, and $\cos\theta^*_{\pi^+}$ is $\approx 1/1.5$ (once a $p_{miss} \leq 0.8$ MeV/c cut is applied) and the $p$-wave signature clearly stands out in the invariant mass bin $600 \leq m_{\pi\pi} \leq 700$ MeV/c$^2$. It is worth noting that the $m_{\pi\pi}$ foreground and background distributions are different, a feature which will be exploited in the $m^*_{\rho^0}$ extraction, in conjunction to the fitting of $\cos\theta^*_{\pi^+}$. These MC-simulated distributions agree very well with TAGX data, under identical conditions (e.g. Fig. 8.

## 5.2 Analysis of the $\pi^+\pi^-p(p)$ Events

In the analysis of the CLAS $\pi^+\pi^-p(p)$ events, the simultaneous detection of one or more nucleons will allow us to place even more stringent conditions, once again effectively enhancing the $\rho^0$ channel. In the case of $\pi^+\pi^-pp$ detection, the reaction

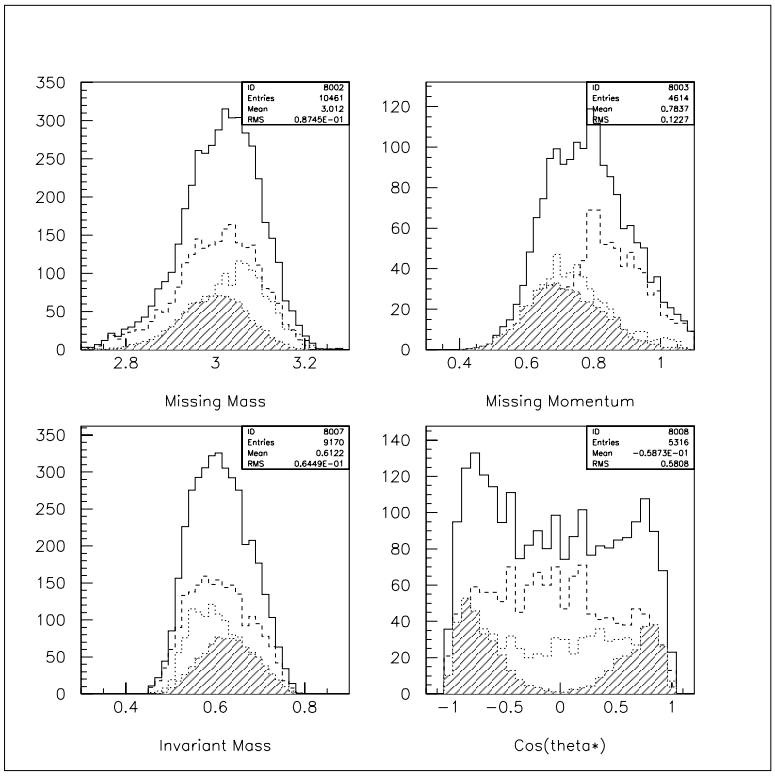


Figure 10: The MC simulated $\pi\pi$ distributions from the $\Delta\pi$ (short-dashed) and $\Delta\Delta$ (long-dashed), respectively, and the foreground reaction $\rho^0 \rightarrow \pi^+\pi^-$, indicated by the shaded area. The solid line represents the total yield of the three reactions. The $\rho^0$ mass was assumed to be 650 MeV/c$^2$. All panels display $\pi^+\pi^-$ events detected in CLAS subject to the cuts indicated in Sections 4.2.1 and 4.2.2. An additional cut on missing mass ($2.9 \leq m_{miss} \leq 3.1$ MeV/c$^2$) has been imposed on the missing momentum ($p_{miss}$), invariant mass ($m_{\pi\pi}$), and $\cos\theta^*$ panels.

is kinematically complete, which further constrains the MC fitting exercise. Here, coplanarity criteria can be employed, which are defined as:

$$(\vec{p}_\gamma \times \vec{p}_p) \cdot (\vec{p}_{\pi^+} + \vec{p}_{\pi^-}) \tag{6}$$

$$(\vec{p}_\gamma \times \vec{p}_p) \cdot (\vec{p}_{\pi^+} - \vec{p}_{\pi^-}) \tag{7}$$

$$(\vec{p}_\gamma \times \vec{p}_{\pi^+}) \cdot (\vec{p}_p \times \vec{p}_{\pi^-}). \tag{8}$$

For events coming from vector meson production on a single nucleon, we expect the angle defined by equation (6) to be a peak centered at 90°, with a width determined from the superposition of the Fermi momentum distribution of single protons in $^3He$ and the experimental resolution. For competing multi-nucleon background processes, this correlation is much weaker and is shown in Fig. 11.

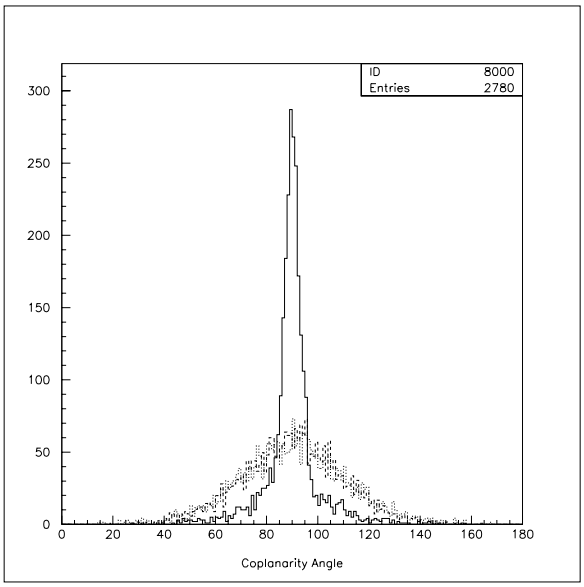


Figure 11: Coplanarity angle, from equation (6), for $\pi^+\pi^-p$ events. The solid line is for the $\rho^0$ production reaction, the dotted line is for the $\Delta\Delta$ reaction and the dashed line is for the FSI affected process.

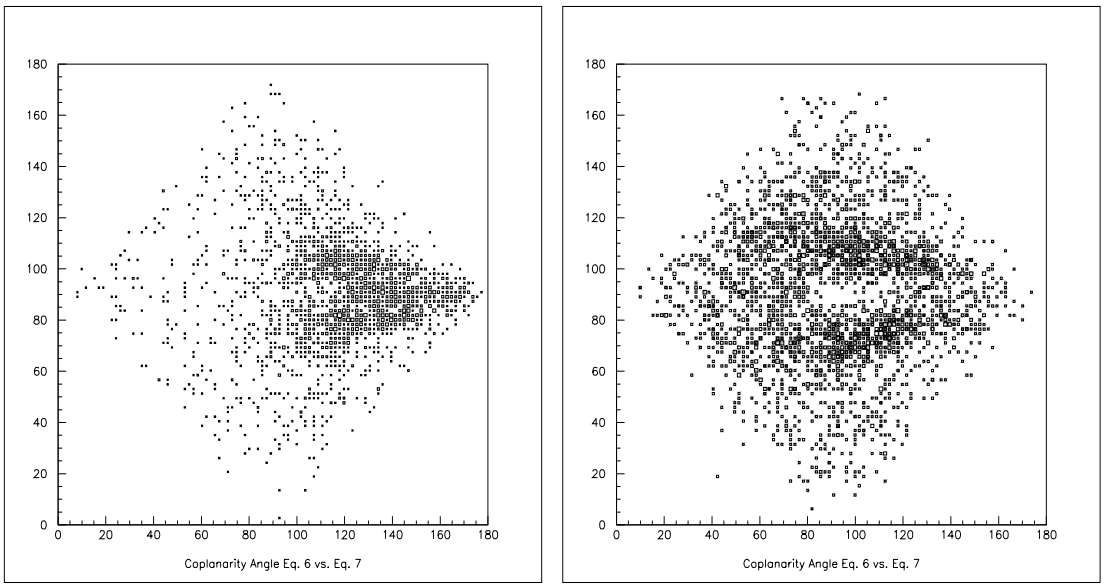


Figure 12: Coplanarity Angles for $\pi^+\pi^-p$ events. The coplanarity angle calculated from equation (7) versus that of equation (8) for the $\rho^0$ production reaction in the left panel (a), and quasifree $N^*$ plus single $\Delta$ reactions in the right panel (b), respectively. A cut around the heart-shaped locus, in panel (a), would preferentially select $\rho^0$ events.

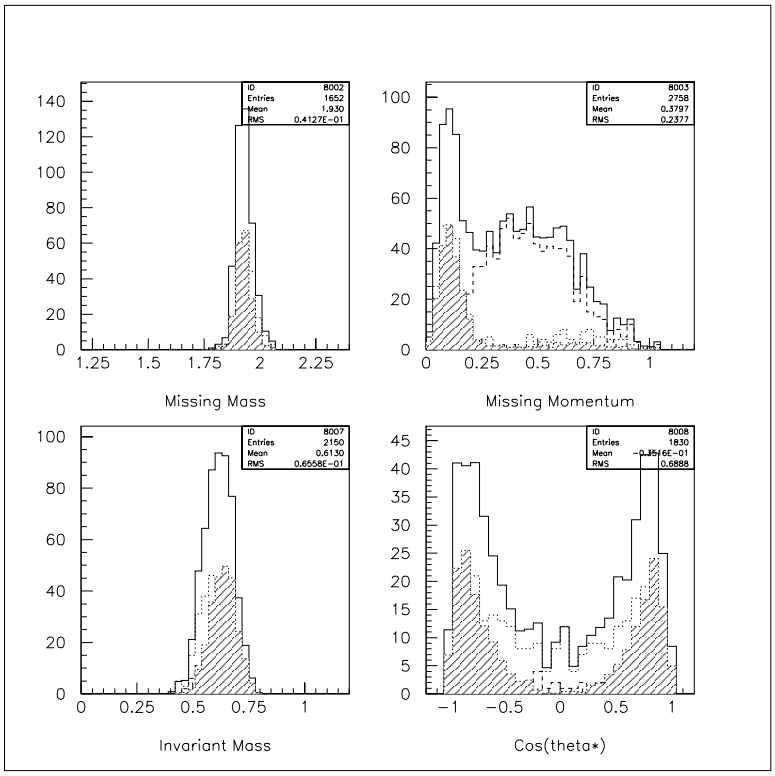


Figure 13: As in Fig. 10, with two additional cuts imposed: one is the coplanarity correlation condition from Fig. 12, and the other is a missing momentum cut applied on the missing mass, invariant mass, and $\cos\theta^*$ panels.

The combined information from equations (7) and (8) can be used as a filter in the analysis to separate the $\rho^0$ from the quasifree $N^*$ and single-$\Delta$ processes. This is illustrated in Fig. 12, where these two coplanarity angles are plotted against one another.

Finally, in Fig. 13 we show the same variables as in Fig. 10, but we now have applied *in addition* the heart-shaped area coplanarity cut from Fig. 12(a), to the background reaction events in panel (b). The missing momentum distribution exhibits the characteristic spectrum of $\Delta\Delta$ due to the second (undetected) nucleon in the reaction. A cut for $p_{miss} \leq 0.22$ GeV/c greatly suppresses this background reaction, resulting in the distributions shown in the other three panels. An extra cut could be also applied from Fig. 11 (area between arrows) to further suppress the $\Delta\Delta$ background, if necessary, but has not been applied in this analysis.

The simulations show that the suppression of background is so effective for the $\pi^+\pi^-p$ data set, that we expect to be able to clearly observe the modified $\rho^0$ peak in the invariant mass spectra, which would further increase the confidence, of an assignment of a value for the modified mass, manyfold over all previous results in

the literature. The final ratio of $F/B \approx 1$ *over all available phase space* is very impressive, considering the initial cross section ratio was $\sigma_{\rho^0}/\sigma_{(\Delta\pi+\Delta\Delta)} \approx 1/18$. **All the emphasis and rates in this proposal are, in fact, based on the $\pi^+\pi^-p$ data-set collection and analysis**. Thus, the importance of the background suppression shown here cannot be overestimated.

### 5.3 Conclusions on Background Reduction

We have shown that, although the cross sections for background reactions producing $\pi^+\pi^-$ pairs far exceed the $\rho^0$ production cross section at subthreshold energies, the unique correlation signatures of the two pions in the $\rho^0 \to \pi^+\pi^-$ decay allow a very effective suppression of the background. This suppression manifests itself on both analysis methods, the MC-based analytical deconvolution of key observables, and the assumption-free $J = 1$ signature of the $\rho^0$. These findings, which are based on CLAS MC simulations for this experiment, are supported by data analysis from TAGX. Furthermore, the suppression of background is accomplished without biasing the $\rho^0$ spectral shapes, by carefully selecting the value of each cut.

## 6 Beam Time Request

In this section, we outline the assumptions and scientific requirements that have been used to calculate the amount of beam time required to accomplish our objectives. As expected, this section relies heavily on input from several sections in this proposal, and these are so identified.

*The final beam time request reflects the emphasis of the proposal on the $\pi^+\pi^-p$ channel, which affords the best quality data based on the CLAS Monte Carlo simulations and the $F/B$ ratio of unity from Section 5.*

### 6.1 Beam Time Calculations

The photon flux from Table 4 is spread over a 1200 MeV-wide bite, and we have scaled it to the 20 MeV-wide bin, assuming a flat distribution of photons in this tagging energy region. We have also assumed an average cross section of $\sigma = 4\ \mu b$, for a modified mass $m^*_{\rho^o}$= 600 MeV/c$^2$ at 800 MeV, which is consistent with the analyses of references [32, 33] and is shown in Fig. 6. The cross sections for $\omega$ and $\phi$ have been normalized to that of the $\rho^0$, by assuming the cross section ratios derived from photoproduction on the proton for $\rho^0$, $\omega$ and $\phi$ scale similarly in the subthreshold region. This results in $\sigma_\omega = 0.44\ \mu b$ and $\sigma_\phi = 0.11\ \mu b$, respectively. This assumption requires an additional correction factor, since the $\omega$ and $\phi$ decay fractions inside the nuclear medium are smaller.

The beam time, $t$, required under the assumptions and criteria above, is calculated using the following relation:

$$\sigma = N_{\rho^0}/[R_\gamma \cdot t \cdot \epsilon \cdot \eta \cdot N_{nuc} \cdot \alpha] \quad (9)$$

where $N_{nuc} = 2 \times 10^{23}$ nuc/cm$^2$ and $R_\gamma = 1.7 \times 10^5 \gamma/s$, are the number of target nuclei and photon flux, respectively, in a 20 MeV wide photon energy bin. The number of *modified* $\rho^0$ events surviving all the cuts is $N_{\rho^0} = 10{,}000$, and the branching ratio for the particular decay is represented by the variable $\alpha$. In this estimate, we have used the acceptance of the $\pi^+\pi^- p$ channel at $E_\gamma$= 800 MeV ($\epsilon = 0.12$, Fig. 5), which was calculated for $m^*_{\rho^o}$= 600 MeV/c$^2$. Furthermore, we have determined that the efficiency of survival of the different offline cuts ($\theta_{\pi\pi}$, coplanarity, $p_{miss}$, $p^*_T$ *vs* $\cos\theta^*_{\pi^+}$, and $m_{miss}$) from Section 5, is $\eta = 0.5$ for the $\rho^0$.

From the above equation, we determine the **beam time required is 420 hours**. It should be emphasized that, at the same time, the number of *medium modified* $\omega$ ($\phi$) mesons detected via the $\pi^+\pi^-\pi^0$ channel, will be approximately 100 (6), under the same $E_\gamma$ binning. Thus, the beamtime on target calculated for the $\rho^0$ (our primary objective), is the minimum beam time required for a serious effort on the $\omega$ and a conclusive feasibility study for the $\phi$. The $\omega$ and $\phi$ events will clearly need coarser $E_\gamma$ and invariant mass binning, but unless their widths are increased in the medium, only a few modified $\phi$ mesons are expected to be observed. On the other hand, the narrow widths of these two mesons and the lack of competing processes, will allow a good confidence level even for small number of modified $\omega$ and $\phi$ signatures. This amount of beam time will also assure a well populated sample of $\pi^+\pi^-$ events coming from the exclusive $\rho^0$ production on $^3He$.

### 6.2 Beam Time Request

*We request 420 hours for $^3$He running in Hall B with the CLAS magnetic field at +0.25B$_\circ$, two-charged-particle trigger, and $E_\gamma$=320-1520 MeV. This estimate does not include data acquisition dead time, neither CEBA nor Hall B beam delivery inefficiencies. 150 hours can be collected in parallel within the already approved* g3 *beamtime and we request* **explicit approval** *to define the operational parameters (torus field and trigger) and to analyze this portion of the* g3 *data. This reduces the number of* **additional beamtime** *requested for this experiment to 270 hours.*

## 7 Conclusions

Subthreshold photoproduction of vector mesons off nuclei is the most precise and promising method of investigating mass modifications in the presence of hadronic matter. Unlike the heavy ion results from CERN, where only invariant mass distributions of dilepton production were considered in the analysis, the experiment in this proposal will analyze several additional sensitive variables simultaneously, which effectively constrain the interpretation of the results. The hadronic decay channel has the advantages of large branching ratios, good final foreground to background

ratio, and it carries information inherent to the $\rho^0$ meson, via its spin in the $l = 1$ signatures in the angular distributions. The $\rho^0 - N$ origin of large mass modifications reported by the TAGX collaboration and the subject of possible bound states for vector mesons in nuclei, can only be probed effectively by such a subthreshold production experiment. Finally, the selection of $^3He$ as our target, together with the multi-observable analysis, minimizes FSI interactions, which could interfere with the sought-for modification signatures.

The experience from the TAGX analysis, coupled with the intrinsic advantages of CLAS and the extensive MC simulations in this proposal, clearly show that the **$\rho^0$ signal can be successfully extracted from the background generated by other processes**. This is a crucial point, since the $\rho^0 \to \pi^+\pi^-$ decay channel provides a unique method with which to investigate medium modifications in light nuclei, coupled to the subthreshold production advantages.

Even though the TAGX results point to an unexpectedly large mass reduction for the $\rho^0$, several important questions are still unanswered and some new ones have been brought forward and which can only be answered by the proposed experiment.

- **Precision of expected CLAS data:** The quality and quantity of the CLAS data will be so much better than those from the TAGX experiment, that we expect to provide a definitive and precise $m^*_{\rho^o}$ measurement, and the results will serve as valuable input to theoretical models in terms of the vector meson mass dependence as a function of hadron density. They will also help decide which, of all the theoretical works, is worth pursuing further.

- **Separation of mass and width modifications:** The TAGX experiment could not make firm conclusions on the relative roles that the mass and/or width modifications play. The proposed measurements will provide conclusive results for the $\rho^0$ because of the more surgical nature of the analysis, especially in connection to the pion emission angle (the $l = 1$ signature) in the dipion center of mass, afforded by an invariant mass binning of 50 MeV/c$^2$ or better. The CLAS out-of-plane acceptance and the analysis of three-track events will be instrumental in this effort.

- **The $\rho^0 - N$ and $\rho^0 - A$ origins of medium modifications:** The separation of the effects on mass and width for the $\rho^0$ in the exclusive and breakup reactions, respectively, with increased statistics and confidence, may provide answers to the questions raised both by the TAGX results and several theoretical expectations. Namely, do we indeed observe a large mass modification due to elements in the $\rho^0 - N$ interaction, which is possibly masking the weaker nuclear effect?

- **Bound $\omega$ states in $^3He$:** This very recent issue greatly affects our understanding of nuclear physics. A bound vector meson state is a direct signature of deep scalar fields which are intrinsic to *QHD*, and the subthreshold production of the $\omega$ will be the testbed of such assertions. It is beyond doubt that if

the $\omega$ is produced at rest with respect to the nucleus and it becomes bound, the signature of such a bound state will show up very clearly. The background to the $\omega \to \pi^+\pi^-\pi^0$ reaction, either by itself or associated with detection of emitted nucleon(s), is so small that even an in-medium decay fraction of a few percent will be observed with confidence. A bound state, by its very own nature, will result in large in-medium decay fractions, compared to in-flight medium modifications. The difference in nature of these two phenomena will result in different experimental signatures.

- **The modifications for the $\phi$ meson:** Due to long decay length and small expected mass modification due to low strangeness content of the nucleon, as well as low production cross section, the search for $\phi$ modifications is more exploratory in nature. If, however, theoretical calculations which predict large modification of the width of the $\phi$ are accurate, the in-medium decay fraction of the produced $\phi$ mesons will increase substantially. Such an observation is very valuable on its own merit and it becomes even more exciting in combination with the other two vector mesons, due to the strangeness content of the $\phi$. Nevertheless, $\phi$ modifications will be very difficult to extract.

# Appendix - Comparison to E94-002 at Hall B

The approved Hall B experiment E94-002, "Photoproduction of Vector Mesons off Nuclei", is similar in topic to the one proposed here. There are, however, also major differences in both the physics objectives and the methodology.

It is the very nature of the subthreshold energy regime that really sets our proposal apart from E94-002. The mass modification induced by the nucleonic density can only be probed at subthreshold energies. As such, we will investigate this new medium effect, which cannot be probed at higher energies and higher Lorentz boost regimes for the vector mesons. In a similar argument, investigation of postulated vector meson bound states for the $\rho^0$ and $\omega$ mesons are not effectively probed at high $E_\gamma$ regions. However, the nuclear mass modification effect is accessed in a similar way between this proposal and E94-002, but with a totally different methodology. With the TAGX results pointing to a large mass modification, the present proposal is less exploratory and more precision oriented in nature than the earlier E94-002.

The choices of energy range and massive targets in E94-002 bring that experiment in the coherent production regime, which dominates vector meson production. These coherent events can be suppressed to an extent by imposing cuts on -$t$, which, however, also reduce the production cross sections substantially. The detection of the leptonic decay products, has, on one hand, the benefit of allowing the use of heavy nuclei as targets, in order to maximize the probability of vector meson decay within the nuclear target. On the other hand, however, the leptonic channel imposes a severe penalty on the final statistics due to the very low branching ratios and due to the production of $e^+e^-$ pairs via the Bethe-Heitler process, which is also more pronounced for heavier nuclei. The latter process can be suppressed by demanding the detection of the recoil nucleon in the production process, a technique which also suppresses coherent production to a degree. The penalty of this technique is that a further loss of acceptance by almost 50% is imposed.

E94-002, then, will attempt to measure the *nuclear effect* of the vector meson mass modification and as such, it is seeking to determine the same effect as one of the two components of the exclusive reaction in our proposal. In this last respect only, the two approaches are complementary. Each one has its own unique technical problems and each one uses a different approach in probing nuclear medium effects.

# References


[1] DeTar CE, *Quark Gluon Plasma 2*, ed. R. Hwa. Singapore: World Sc. (1995).
K.J. Escola, Nucl. Phys **A590** (1995) 383c.
F. Wilczek, Physics Today, April 1998, p.11.

[2] F. Douglas Swetsy *et al.*, Astro. Phys. Jour. **425** (1994) 195.

[3] M. Prakash *et al.*, Phys. Rep. **280** (1997) 1.

[4] F. Karsch, Nucl. Phys. **A590** (1995) 367c.

[5] T. Hatsuda and T. Kunihiro, Phys. Rep. **247** (1994) 387.

[6] T. Hatsuda, LAMPF preprint nucl-th/9608037.

[7] C.M. Ko, V. Koch and G. Li, Ann. Rev. Nucl. Sci. **47** (1997) 505.

[8] G.E. Brown, M. Buballa and M. Rho, Nucl. Phys. **A609** (1996) 519.

[9] C. Bernard *et al.*, Phys. Rev. **D45** (1992) 3854.

[10] G.E. Brown and M. Rho, Phys. Rev. Lett. **66** (1991) 2720.

[11] T. Hatsuda and S.H. Lee, Phys. Rev. **C46** (1992) R34.

[12] T. Hatsuda, S.H. Lee and H. Shiomi, Phys. Rev. **C52** (1995) 3364.

[13] T. Hatsuda, LAMPF preprint nucl-th/9702002.

[14] X. Jin and D.B. Leinweber, Phys. Rev. **C52** (1995) 3344.

[15] K. Saito and A.W. Thomas, Phys. Rev. **C52** (1995) 2789.

[16] M. Asakawa and C.M. Ko, Nucl. Phys. **A572** (1994) 732.

[17] M. Asakawa and C.M. Ko, Phys. Rev. **C48** (1993) R526.

[18] F. Klingl *et al.*, Nucl. Phys. **A560** (1997) 527.

[19] J.D. Walecka, Theoretical Nuclear and Subnuclear Physics, Oxford University Press (1995).

[20] B.D. Serot and J.D. Walecka, Adv. Nucl. Phys. **16** (1986) 1.

[21] S.J. Wallace, Ann. Rev. Nucl. Part. Sci. **37** (1987) 267.

[22] P.G. Reinhard, Rep. Prog. Phys. **52** (1989) 439.

[23] K. Tsushima *et al.*, LAMPF preprint nucl-th/9806043 (1998).

[24] Z. Papandreou *et al.*, Phys. Rev. **C59** (1999) R1864.

[25] A. Bhattacharyya *et al.*, nucl-th/9902060.

[26] G. Agakichev *et al.*, CERES Collaboration, Phys. Rev. Lett. **75** (1995) 1272.

[27] J.P. Wurm *et al.*, NA45 Collaboration, Nucl. Phys. **A590** (1995) 103c.

[28] M. Masera *et al.*, HELIOS-3 Collaboration, Nucl. Phys. **A590** (1995) 93c.

[29] G.E. Brown et al., Phys. Rev. Lett. **60** (1998) 2723.

[30] E.J. Stephenson *et al.*, Phys. Rev. Lett. **78** (1997) 1636.

[31] K. Maruyama *et al.*, Nucl. Instr. Meth. in Phys. Res. **A376** (1996) 335.

[32] G.J. Lolos *et al.*, Phys. Rev. Lett. **80** (1998) 241.

[33] G.M. Huber, G.J. Lolos and Z. Papandreou, Phys. Rev. Lett. **80** (1998) 5285.

[34] M. Kagarlis *et al.*, LAMPF preprint nucl-ex/9811010, Phys. Rev. C, in press.

[35] N. Bianchi *et al.*, APS preprint nucl-th/9904033.

[36] C. Song, Phys. Rev. **D48** (1993) 1375.

[37] N. Isgur, private communication (1998).

[38] P.-Y. Bertin, M.V. Kossov, B.M. Preedom *et al.*, "Photoproduction of Vector Mesons off Nuclei", JLab Proposal E94-002.

[39] H. Alvensleben *et al.*, Nucl. Phys. **B18** (1970) 333.

[40] K. Saito,T. Tsushima and A.W. Thomas, Phys. Rev. **C55** (1997) 2637.

[41] B.L. Berman, P. Corvisiero, G. Audit *et al.*, "Photoreactions on $^3He$," JLab Proposal E93-044.

[42] K. Saito, T. Tsushima and A.W. Thomas, Phys. Rev. **C56** (1997) 566.

[43] P. Guichon and M. Ericson, private communication.

[44] M.C. Abreu *et al.*, NA38 Collaboration, Nucl. Phys. **A590** (1997) 117c.
M.C. Abreu *et al.*, NA50 Collaboration, Phys. Lett. **B410** (1997) 327, 337.

[45] M. Battaglieri *et al.*, *CLAS-Note* 97-006.

[46] E.S. Smith, "FAST Monte Carlo for CLAS", *CLAS-Note* 90-003.

[47] D. Lüke, P. Söding, Springer Tracts Mod. Phys. **59** (1971) 39.

[48] M. Asai, et al., Zeit. Phys. **A344** (1993) 335.

[49] Y. Wada, representing the SAPHIR collaboration, Particles and Nuclei International Conference, Williamsburg, VA, June, 1996.

[50] D.G. Watts et al., Phys. Rev. C **55** (1997) 1832.